Hindawi
International Transactions on Electrical Energy Systems
Volume 2022, Article ID 8802143, 24 pages
https://doi.org/10.1155/2022/8802143

Research Article

A Coordinated Pumped Storage Dual Compensated Hydro Governor with PSS Action to Damp Electromechanical Power Oscillations

Narayan Nahak and Samarjeet Satapathy

Department of Electrical Engineering, Siksha"O"Anusandhan Deemed to Be University, Bhubaneswar, Odisha, India

Correspondence should be addressed to Narayan Nahak; narayannahak@soa.ac.in

Received 24 March 2022; Revised 19 August 2022; Accepted 26 August 2022; Published 19 October 2022

Academic Editor: Yu-Chi Wu

Subject to increasing penetrations of renewable sources like solar photovoltaic (SPV) and wind energy sources, power system oscillation damping is going to be a critical challenge for system operators. This work proposes a new dual compensated governor (DCG) in coordination with a power system stabilizer (PSS) of a pumped storage hydro plant for power oscillation damping subject to intermittent SPV and wind penetration for a hydro, wind, and SPV integrated power system. The phase lag provided by the hydro governor is compensated by additional phase lead contributed by the dual compensation, where speed and real power deviations brought by uncertain SPV and wind penetrations are simultaneously controlled by two lead-lag controllers before being applied to conventional Proportional-Integral-Derivative (PID) governor. Again, subject to critical oscillatory unstable conditions, the DCG is coordinated with PSS through a multiobjective function employing a new modified Differential Evolutionary-Particle swarm optimization (MDEPSO) algorithm. Different case studies with sudden and random SPV and wind penetrations being executed with the proposed controller considering a two area four machine and 39 bus multimachine system with pumped storage hydro units to observe system oscillations are considered. The proposed damping control action has been implemented to damp these oscillations, and the damped response has been analyzed with eigenvalue distributions and Bode plots with sensitivity analysis. The proposed action is found to be much more efficient in contrast to conventional PID governor and PSS damping action. Also, the usage of present hydro governors can be much improved by this coordinated controller action.

1. Introduction

Renewable power generation (RPG) is going to be an integral part of bulk electric power generation, which includes generation from the hydropower plant (HPP), SPV, wind source, tidal, biomass, etc. [1]. For the integration of RPG, much more effort has been implemented worldwide including new transmission topology or technologies with PV generation [2, 3]. Out of several renewable sources, HPP is an important constituent in power generation sharing to counteract increasing load demands [4]. There are different categories of HPPs, including conventional, run of river, and pumped storage. A conventional HPP employs a dam for storing water. Run of river HPP usually has either no water storing or very less water storing capability. For HPP, proper storing and utilizing of water resources is an important issue for optimal power generation, which can be met by a pumped storage hydropower plant (PSHPP). In PSHPP the water resources can be efficiently utilized by storing the water and pumping as per load demand [5]. PSHPP has different states of operation, which are pumping and generating modes. There are upper and lower reservoirs in PSHPP. In the pumping state, the water is pumped to the upper reservoir from the lower reservoir, where the power demand is less. In the generation state, the water from the upper reservoir is utilized for power generation when the power demand increases. Therefore, PSHPP plays a very important role in power balancing. A battery energy storage system (BESS) is usually employed to meet the challenge of uncertainty and intermittence in RPG integration, like SPV

and wind sources. But there are several drawbacks of BESS, like less current carrying capability of semiconductor switches, lower power handling capability, and short life time [6].

1.1. Literature Review. Due to randomness in SPV and wind generation, electromechanical oscillation (EMO) generated in the power system poses much more challenges to the system operator. In [7], an analysis has been presented depicting the impact of uncertain wind penetration on the stability of the power system. As per [8], the damping capability of wind sources can be imparted if wind turbines run at a constant speed. But as per [9], the small signal stability is a challenging issue with intermittent wind penetration, and the stability depends on the operating condition. The wind and synchronous generator may interact to provide positive or weak damping to EMO [10], and the stability may sacrifice if there is a strong coupling between wind and conventional generation [11]. So as per this research, variable wind integration creates a challenge to damping EMO. In a similar way, varying SPV also poses a challenge to EMO damping. In [12, 13], research have been conducted predicting the impact of undertrained SPV penetration on small signal stability of power system. The contribution to EMO depends on the characteristics of SPV, which have been analyzed in [14, 15]. Sudden and random SPV integration with the power system aggravated EMO [16]. As in [17], the mechanical mode of oscillation is more excited with heavy SPV penetration, and critical machines need to be identified to damp oscillations, which may be a difficult task. Time domain simulation and analysis have been performed in [18] with different RPGs subject to small signal stability, which explained optimal usage of different sources for stability improvement. Also, in [19], it has been observed that undertrained SPV penetration poses challenges for EMO damping. Therefore, as per the research stated above, damping EMO is a critical challenge for system operators when there are uncertain SPV and wind penetrations. A power system stabilizer (PSS) is usually employed to dampen EMO, which creates an electrical damping torque in the generator through an excitation system [20]. In [21], a criterion has been developed for selecting an optimal node to install PODs and PSSs, but the setting of parameters of the damping controller and its impact can be studied further. So, an important issue is selecting the proper PSS controller. The PSS control action may hamper regulating voltage and provides leading pf, which are demerits of PSS controller. Again, in the current state of deregulation in the power sector the optimal use of existing resources like mechanical torque control imparted by generator governor action would be an efficient technique if the governor's performance is improved. In [22], the efficiency of turbine governor action for oscillation damping has been presented, where it has been shown that speed control and excitation loop may be decoupled and do not influence each other. The governor can efficiently provide mechanical torque to stabilize frequency [23], but there may be a modification in turbine governor performance if additional phase compensation is provided with the governor [24]. But in the report of [25], it has been presented that hydro governors are generally blocked to damp interarea oscillation. So, although the governor can impact damping torque, its controllability needs to be improved much to counteract low interarea oscillations. The governor parameters need to be tuned efficiently to provide adequate damping torque. If steam valve control and excitation control are coordinated, then the control action would be enhanced as reported in [26], but using an efficient optimization technique may reduce a detailed mathematical model for efficient control action. In the current and future content of power system, HPP is going to take an important role so there can be a modification in hydro turbine governor action along with proper coordination by excitation system provided by PSS. This attempt has been performed in this work where the turbine governor action is coordinated with PSS to create damping torque with randomly changing loads, uncertain renewable penetration, varying operating condition, several disturbances, and interconnection of the power system network. The modern power system is going to face a lot of challenges penetrating to damping of EMO. Hence for optimal usage of turbine governor control to meet these challenges, a new modification in governor control action is performed in this work, in coordination with PSS action. Usually, the input to the governor is speed deviations, but if real power deviation can also be given simultaneously with additional phase compensation, the performance of the governor would be much enhanced. In this work, the hydro turbine governor is given dual inputs, which are speed and real power deviation, and both are fed simultaneously through different phase lead compensation which has been named here as dual compensated governor (DCG). The next aspect is setting control action gains optimally to enhance controller efficacy. In this context, currently, much research have been performed on advanced optimization processes. In [27], a low computational burden model predictive control based on a social ski driver algorithm has been presented for intelligent vehicular applications. In [28], arithmetic optimization algorithm (AOA) tuned model predictive control paradigm is proposed for automatic voltage regulators against uncertainty. So, on lightning search algorithm has been applied for variable structure control for a nuclear reactor power system in [29]. Whale optimization algorithm has been applied in [30] in contrast to other metaheuristics to design a new robust control method for wind energy conversion systems. Different researchers also have investigated the impact of a suitable control action and appropriate algorithm to regulate frequency in a power system. Genetic algorithm tuned fuzzy gain scheduling controller and optimal regulator are proposed in [31, 32] and an integrating layered recurrent ANN-based control action is proposed in [33] with various operating conditions including DFIG-based wind energy integration for automatic generation control. The system dynamic response can be regulated and improved with an energy storage device like a redox flow battery and an appropriate controller like fuzzy PID action as reported in [34], where the controller parameters are tuned with the SSA algorithm. In this work, different nonlinearities that

resembled real world systems are also included to justify the control action. The coyote optimization algorithm is proposed in [35] with a fuzzy controller to improve frequency stability along with wind turbine units. Metaheuristic algorithms are justified to be much more efficient for handling different optimization problems, as reported by researchers. For this work, a new hybrid modified DE with PSO technique is proposed. DE and PSO are efficient evolutionary and swarm control laws being employed by many researchers for optimization. But, in contrast to DE, modified DE can choose suitable F and CR at the time of the program run, which exponentially decays from 1 to 0.01 and speeds up the computational time [36]. Due to lack of storage in MDE, the result may be local optima, which is the demerit of MDE. PSO provide a global best value and cover up the storage problem and can be easily implemented. Hence hybrid MDEPSO optimization technique has been developed here including the merits of both DE and PSO. This algorithm has been tested with some standard benchmarks.

1.2. Research Gap and Motivation. The research gap identified by the author is that hydro governors are under usage to damp EMO which is an important concern for modern power system networks subject to uncertain penetrations of renewable sources. Though researches focus on the utilization of the governor for frequency control still, there is not much for EMO damping as per the author knowledge. In [37], eigen analysis has been performed for hydraulic, mechanical, and electrical coupling systems but optimal coordinated control of the system may improve system dynamic response with modification in control action provided by the governor and PSS. For a modern power system, hydro plant is going to be an indispensable energy source; especially pumped storage units provide an additional advantage of addressing energy storage problems and challengeable to battery energy storage systems. But, the varying penetrations of renewable like solar and wind sources give rise to electromechanical oscillations in the power system, which need to be damped at an earlier stage, or else may lead to eventual loss of synchronism. So, to address this issue, a variable renewable penetrated PSHP dominated power system is considered in this work. Here the PSHP governor is modified with a dual compensated network and coordinated with PSS by a control strategy to impart an effective damping torque for power oscillations brought by random changes in solar and wind outputs. By this action, the utilization of governor action would be much improved so as to tackle critical oscillations in the power system. The prime contribution of the present work is a modification in PSHPP governor with PSS and coordination between them to handle electromechanical oscillations in power systems even to the critical oscillatory condition due to renewable penetrations. Also, the traditional governor needs to be much improved to provide effective damping torque for critical oscillations.

1.3. Research Contribution. As per the reviews of literature mentioned in previous sections, hydro governors need to be modified in contrast to existing models to counteract critical oscillatory conditions. In this model, compensation networks are implemented in the path of speed and real power signals to impart effective damping torque by the governor. Also, as per existing works, PSS are not properly coordinated so as to handle critical system oscillations, but in this model, PSS have been coordinated with a modified governor so that sufficient damping torque can be contributed for system oscillations. So, the proposed approach can enhance the effective damping torque contribution of both the governor and PSS.

The prime contribution of this work can be stated in brief as follows:

(i) A new dual compensated pumped storage hydro governor (DCG) is proposed.

(ii) A new coordinated control of DCG with PSS is proposed for efficient damping torque contribution.

(iii) Intermittent and sudden SPV/wind penetration is executed to observe electromechanical low frequency oscillations and proposed control action being implemented to damp oscillations.

(iv) A new hybrid modified DE with PSO is proposed to tune control action parameters.

(v) This control action can prevent underutilizing governor action to dampen EMO as well as enhance the efficacy of pumped storage hydro plant.

1.4. Paper Organization. The rest part of this manuscript has been organized as follows: Section 2 presents the modeling of PSHPP with PSS and governor action, Section 3 illustrates modified governor and proposed control action, Section 4 describes the multiobjective function and proposed optimization technique. The case studies and analysis with proposed control action are presented in Section 5 and the conclusion in the conspectus is presented in Section 6.

2. Modeling of PSHPP with PSS and Governor Action

The PSHPP has an upper and a lower reservoir and can meet the requirement of energy storage. It can operate in generating or pumping mode. Generating mode is initiated for high energy demand and the pumping mode is for low energy demand. When demand for energy is less, the PSHPP turbine works in pumping mode, thereby pumping water from the low to the upper reservoir, and so, during the hereby demand of energy period, the turbine works in generating mode thereby utilizing upper reservoir water for generation purpose so as to meet the load. Figure 1 depicts a PSHPP connected to the grid.

2.1. PSHPP Modeling with PSS. The hydro generator is modeled here in terms of transfer function pertained to small signal analysis, where K_1 to K_6 are constants of the generator model dependent on operating conditions [19]. The real power, output voltage, and field emfs can be presented by the following equations:

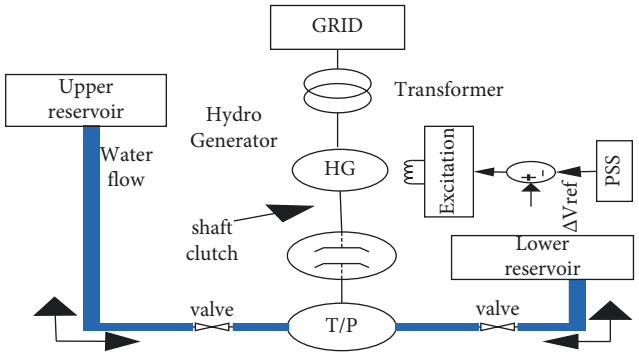

Figure 1: PSHPP with PSS.

$$\Delta P_e = K_1\Delta\delta + K_2\Delta E_q', \tag{1}$$

$$\Delta E_q = K_4\Delta\delta + K_3\Delta E_q', \tag{2}$$

$$\Delta V_t = K_5\Delta\delta + K_6\Delta E_q'. \tag{3}$$

The linearized equation of the machine is given below:

$$\Delta\dot{\delta} = \omega_0\Delta\omega, \tag{4}$$

$$\Delta\dot{\omega} = -\frac{K_1}{M}\Delta\delta - \frac{D}{M}\Delta\omega - \frac{K_2}{M}\Delta E_q' + \frac{\Delta P_M}{M}, \tag{5}$$

$$\Delta\dot{E}_q' = -\frac{K_4}{T_{d0}'}\Delta\delta - \frac{K_3}{T_{d0}'}\Delta E_q' + \frac{\Delta E_{\text{fd}}}{T_{d0}'}, \tag{6}$$

$$\Delta\dot{E}_{\text{fd}} = -\frac{K_5K_a}{T_a}\Delta\delta - \frac{K_6K_a}{T_a}\Delta E_q' - \frac{\Delta E_{\text{fd}}}{T_a} + \frac{\Delta V_{\text{pss}}K_a}{T_a}, \tag{7}$$

$$\Delta\dot{V}_1 = -K_1K_{\text{ps}}\Delta\delta - DK_{\text{ps}}\Delta\omega - K_2K_{\text{ps}}\Delta E_q' + K_{\text{ps}}\Delta P_m - \frac{\Delta V_1}{T_W}. \tag{8}$$

The PSS is connected through an excitation system to the generator and change in PSS output voltage is depicted by ΔV_{pss} by equation (9), where K_{ps}, T_1, T_2 are PSS tuning parameters.

$$\begin{aligned}\Delta\dot{V}_{\text{pss}} = &-\frac{K_1K_{\text{ps}}T_1}{T_2}\Delta\delta - \frac{DK_{\text{ps}}T_1}{T_2}\Delta\omega - \frac{K_2K_{\text{ps}}T_1}{T_2}\Delta E_q' \\ &+ \frac{K_{\text{ps}}T_1}{T_2}\Delta P_M + \frac{\Delta V_1}{T_2}\left(1 - \frac{T_1}{T_W}\right) - \frac{\Delta V_{\text{pss}}}{T_2}.\end{aligned} \tag{9}$$

Governor $\Delta\omega_{\text{ref}}$ and ΔP_{eref} are not considered here. The gate opening ΔY can be presented by Equation (10). ΔY_1, and ΔY_2 are outputs of the integrator and servo system. ΔX_1, ΔX_2 are integral and derivative outputs. The governor dynamics are presented by the following equations [38] in the required form:

$$\Delta\dot{Y} = \frac{\Delta Y_1 - \Delta Y}{t_a}, \tag{10}$$

$$\Delta\dot{Y}_1 = K_{\text{sm}}\Delta Y_2, \tag{11}$$

$$\begin{aligned}\Delta\dot{Y}_2 = &\frac{K_1K_pK_CR_P}{T_C}\Delta\delta - \frac{K_pK_C}{T_C}\Delta\omega + \frac{K_2K_pK_CR_P}{T_C}\Delta E_q' \\ &+ \frac{K_C}{T_C}\Delta X_1 + \frac{K_C}{T_C}\Delta X_2 - \left(\frac{K_C}{T_C}\right)\Delta Y - \frac{\Delta Y_2}{T_C},\end{aligned} \tag{12}$$

$$\Delta\dot{X}_1 = K_1R_PK_i\Delta\delta - K_i\Delta\omega + K_2K_iR_P\Delta E_q', \tag{13}$$

$$\begin{aligned}\Delta\dot{X}_2 = &\left(\frac{K_1K_d}{MT_d} - \frac{K_2K_4R_PK_d}{T_{\text{do}}'T_d}\right)\Delta\delta + \left(\frac{D}{M}\frac{K_d}{T_d} + \frac{R_PK_dK_1\omega_0}{T_d}\right)\Delta\omega \\ &+ \left(\frac{K_2K_d}{MT_d} - \frac{K_2K_3R_PK_d}{T_{\text{do}}'T_d}\right)\Delta E_q' + \frac{K_2R_PK_d}{T_{\text{do}}'T_d}\Delta E_{fd} - \frac{K_d\Delta P_m}{MT_d} - \frac{\Delta X_2}{T_d}.\end{aligned} \tag{14}$$

Taking the length of penstock as L (cm), *c. s* area (m^2), water discharge q (m^3/sec), and static head h_s (m), the discharge rate is given by equation (15) and in pu in equation (16):

$$\frac{dq}{dt} = \frac{\left(h_s - h - h_p\right)gA}{L}, \tag{15}$$

$$\frac{dq}{dt} = \frac{\left(1 - h - h_p\right)}{T_{\text{tw}}}, \tag{16}$$

where T_{tw} is water time constant given by equation (17) and the output prime mover power is presented by equation (18) on the MVA base of the hydro generator.

$$T_{tw} = \left(\frac{L}{A}\right)\left(\frac{q_b}{h_b g}\right), \tag{17}$$

$$P_m = A_t h(q - q_n) - D_t Y_0 \Delta\omega, \tag{18}$$

$$A_t = \frac{(\text{Turbine MW rating})}{(\text{Generator MVA rating})} h_{\text{rated}}(q_{\text{rated}} - q_n). \tag{19}$$

The linearized prime mover output power are given in the following:

$$\Delta P_m = \frac{A_t(1 - Z_1 s)}{(1 - Z_2 s)} \Delta Y - D_t Y_0 \Delta\omega, \tag{20}$$

where $Z_1 = (q_0 - q_n)/T_{tW}$,, $Z_2 = Y_0 T_{tW}/2$.

The transfer function of the linearized turbine is given by equation (21) by taking $Y_0 = q_0$ and neglecting the damping coefficient.

$$G_T = \frac{\Delta P_m}{\Delta Y} = \frac{1 - Y_0 T_{tW} s}{1 + (Y_0 T_{tW} s/2)} \times A_t, \tag{21}$$

$$\begin{aligned}\Delta \dot{P}_m &= \frac{D_t Y_0}{M} K_1 \Delta\delta + D_t Y_0 \left(\frac{1}{Z_2} + \frac{D}{M}\right)\Delta\omega + \frac{D_t Y_0 K_2}{M} \Delta E_q^{'} \\ &\quad - \left(\frac{D_t Y_0}{M} - \frac{1}{Z_2}\right)\Delta P_m - \frac{A_t}{Z_2}\left(1 + \frac{Z_1}{t_a}\right)\Delta Y \\ &\quad - A_t \frac{Z_1}{Z_2 t_a} \Delta Y_1.\end{aligned} \tag{22}$$

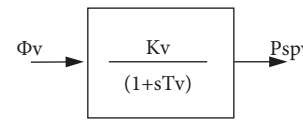

Figure 2: Modeling of SPV generation.

2.2. Modeling of SPV and Wind Energy Generation. P_{spv} is SPV generation in watt can be presented as follows [18]:

$$P_v = P_{\text{spv}} = \eta_c S_a \phi_v [1 - 0.005(T_a + 25)], \tag{23}$$

Here P_{spv} depends on T_a and ϕ_v, which are temperature and radiation and η_c and S_a are constants, which are efficiency and area. Temperature T_a is taken as 25°C. Figure 2 shows the SPV modeling.

For wind energy generation, the natural wind speed is employed to rotate the turbine. The speed of rotation of the shaft is raised by gear box. The wind mechanical energy is transformed into electrical energy through the grid and fed to transformers.

Models of wind speed: the different wind types are classified as random, gradient, gusty, and basic types [18].

Random type: here, Gaussian noise is employed to express the random speed of the wind as given by the following equation:

$$V_R = 2 \sum_{i=1}^{N} \sqrt{S_R(\omega_i)\Delta\omega_w} \cos(\omega_i + \phi_i), \tag{24}$$

$$\begin{cases} \omega_i = (i - o.5)\Delta\omega_w, \\ S_R(\omega_i) = \dfrac{2K_N F^2 |\omega_i|}{\prod^2 \sqrt[4]{\left(1 + \left(F_{\omega_i}/\mu\prod\right)^2\right)^3}}. \end{cases} \tag{25}$$

Gradient wind can be expressed as follows:

$$V_G = \begin{cases} 0, t \langle T_{\text{Gs}}, V_{G,\max} \dfrac{t - T_{\text{Gs}}}{T_{G1}}, T_{\text{Gs}} \le t \le T_{\text{Gs}} + T_{G1}, V_{G\max}, T_{\text{Gs}} + T_{G1} \le t \le T_{\text{Ge}} - T_{G2}, \\ V_{G,\max} \dfrac{T_{\text{Ge}} - t}{T_{G2}}, T_{\text{Ge}} - T_{G2} \le t \le T_{\text{Ge}}, \\ 0, t > T_{\text{Ge}}. \end{cases} \tag{26}$$

Gusty wind can be expressed as follows:

$$V_s \begin{cases} 0, t < T_{\text{is}}, \\ \dfrac{V_{s\max}}{2}\left(1 - \cos\left(2\prod \dfrac{t}{T_{\text{Se}} - T_{\text{Ss}}} - \dfrac{T_{\text{SS}}}{T_{\text{Se}} - T_{\text{SS}}}\right)\right), 0, t > T_{2s}. \end{cases} \tag{27}$$

Equation (28) shows the wind turbine power output as presented by the following:

$$P_w = \left(\frac{1}{2}\right)\rho_d A_b C_p V_W^3, \tag{28}$$

where P_{w} varies with $\rho_d = 1.25$ kgm^{-3} and $A_b = 1735\,\text{m}^2$, which are the density of air and sweeping blade area, respectively. V_{W} in ms^{-1} is the velocity of wind, which depends on $C_{p,}$ which varies with λ_p and $\beta_{p,}$ which are tip ratio and

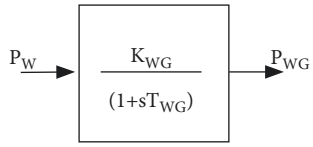

Figure 3: Modeling of wind generation.

blade pitch angle, respectively. Blade radius and speed are 23.5 m and 3.14 rads$^{-1,}$ respectively. C_p is given by the following:

$$C_P = \left(0.44 - 0.0167\beta_p\right)\sin\left[\frac{\pi\left(\lambda_p - 3\right)}{15 - 0.3\beta_p}\right] - 0.0184\left(\lambda_p - 3\right)\beta_p, \tag{29}$$

Figure 3 represents the output power in pu versus V_W and model of wind power generation, respectively. This model is given by the following:

3. Modified Governor and Proposed Control Action

Generally, the governors are not associated with interarea oscillation damping because their parameters are not set properly [25]. So, to enhance the usefulness of conventional

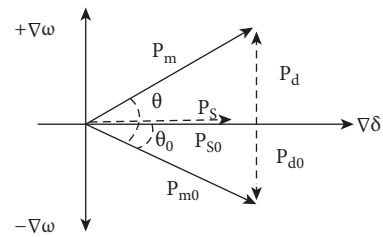

Figure 4: Phasor diagram of governor torque.

hydro governor, a modification is proposed in the present work. The dynamics of conventional governor provide negative damping to oscillations, and the system eigenvalues are shifted to the right half of s-plane. Hence as a remedy to this, a damping torque can be created by the governor if a signal in phase with angular rotor frequency variations is applied. As shown in Figure 4 the mechanical power P_{m0} is shifted to P_{m} and the damping component shifted to P_d from P_{do}, thereby creating a +ve damping torque. In this work, the input to the governor is both speed and electrical power deviation signal. In dual controlled governor, two simultaneously controlled phase compensation networks are inserted in parallel with the speed and real power variation signals, as shown in Figure 5, where the PID governor is supplemented by dual phase compensation network.

$$\Delta\dot{C}_3 = \left(-\Delta\omega - \Delta C_3\right)\frac{1}{0.05}, \tag{30}$$

$$\Delta\dot{C}_2 = -\Delta\omega\frac{K_w}{0.05} - \frac{\Delta C_2}{T_W} - \Delta C_3\frac{K_w}{0.05}, \tag{31}$$

$$\begin{aligned}\Delta\dot{C}_1 = {} & -\Delta\omega\frac{T_{p1}}{T_{p2}}\frac{K_w}{0.05} - \Delta C_3\frac{T_{p1}}{T_{p2}}\frac{K_w}{0.05} \\ & -\left(\frac{1}{T_W}\frac{T_{p1}}{T_{p2}} + \frac{1}{T_{p2}}\right)\Delta C_2 - \frac{1}{T_{p2}}\Delta C_1,\end{aligned} \tag{32}$$

$$\begin{aligned}\Delta\dot{U}_2 = {} & -\frac{K_2K_4K_{\mathrm{pe}}}{T'_{\mathrm{do}}}\Delta\delta + K_pK_1\omega_0\Delta\omega - \frac{K_3K_{\mathrm{pe}}K_2}{T'_{\mathrm{do}}}\Delta E'_q \\ & + \frac{K_{\mathrm{pe}}K_2}{T'_{\mathrm{do}}}\Delta E_{\mathrm{fd}} - \frac{\Delta U_2}{T_W},\end{aligned} \tag{33}$$

$$\begin{aligned}\Delta\dot{U}_1 = {} & -\frac{K_{\mathrm{pe}}K_2K_4}{T'_{\mathrm{do}}}\frac{T_{e1}}{T_{e2}}\Delta\delta + K_{\mathrm{pe}}K_1\omega_0\frac{T_{e1}}{T_{e2}}\Delta\omega - \frac{K_{\mathrm{pe}}K_2K_3}{T'_{\mathrm{do}}}\frac{T_{e1}}{T_{e2}}\Delta E'_q \\ & + \frac{K_{\mathrm{pe}}K_2}{T'_{\mathrm{do}}}\frac{T_{e1}}{T_{e2}}\Delta E_{fd} - \frac{\Delta U_1}{T_{e2}} + \frac{\Delta U_2}{T_{e2}}\left(\frac{T_{e1}}{T_W} + 1\right),\end{aligned} \tag{34}$$

$$\begin{aligned}\Delta\dot{Y}_2 = {} & \frac{K_CK_p}{T_C}\Delta C_1 - \frac{K_CK_pR_P}{T_C}\Delta U_1 + \frac{K_C}{T_C}\Delta X_1 + \frac{K_C}{T_C}\Delta X_2 \\ & - \Delta Y\left(\frac{K_C}{T_C}\right) - \frac{1}{T_C}\Delta Y_2,\end{aligned} \tag{35}$$

$$\Delta\dot{X}_1 = K_i\Delta C_1 + R_PK_i\Delta U_1, \tag{36}$$

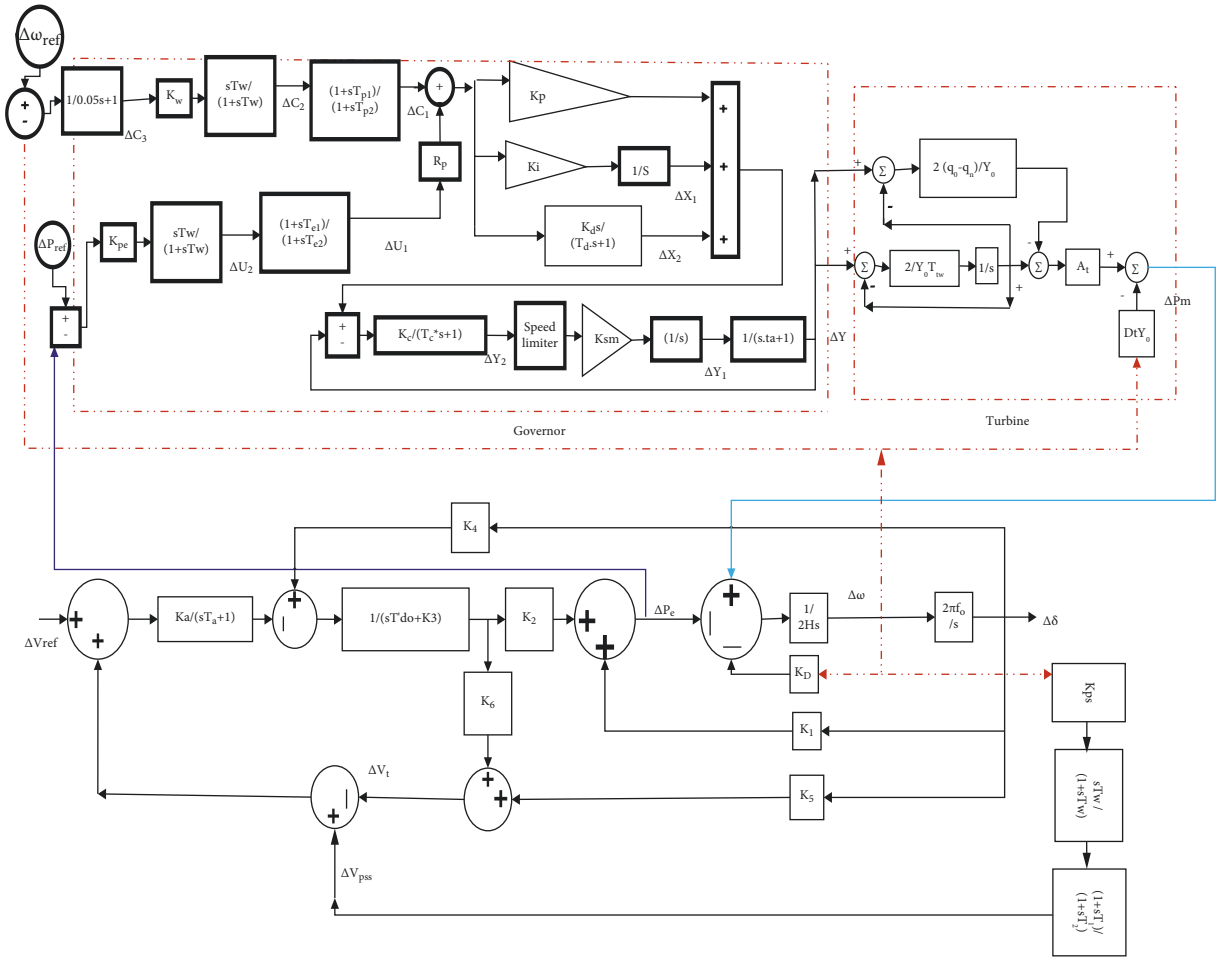

Figure 5: Small signal model of PSHPP with proposed control action.

$$\begin{aligned}\Delta\dot{X}_2 &= \frac{K_d}{T_d}\left(\frac{T_{p1}}{T_{p2}}\left(\frac{K_w}{0.05}\left(-\Delta\omega-\Delta C_3\right)-\frac{\Delta C_2}{T_W}\right)+\Delta C_2-\Delta C_1\right)\\&+\frac{R_P K_d}{T_d}\left(\left(K_{\mathrm{pe}}\left(K_1\omega_0\Delta\omega+K_2\frac{\Delta E_{fd}}{T'_{\mathrm{do}}}-\frac{K_2}{T'_{\mathrm{do}}}\left(K_4\Delta\delta+K_3\Delta E'_q\right)\right)-\frac{\Delta U_2}{T_W}\right)\frac{T_{e1}}{T_{e2}}+\frac{\Delta U_2}{T_{e2}}-\frac{\Delta U_1}{T_{e2}}\right)\\&-\frac{\Delta X_2}{T_d}.\end{aligned}\tag{37}$$

In the above equations, ΔC_1,ΔC_2&ΔC_3 are the lead-lag compensator, washout block& delay outputs, respectively, for angular speed variation, which is given in equations (30)–(32). ΔU_1&ΔU_2 are the lead-lag compensator & washout block outputs, respectively, for real power variations, which are given in equations (33)–(34). Modification of ΔY_2, ΔX_1&ΔX_2 due to DCG are given in equations (35)–(37).

Figure 5 shows the proposed control action with turbine and synchronous generator small signal modeling. In the proposed controller, dual compensated governor (DCG) and PSS are coordinately tuned and the strategy of coordination is presented in Figure 6. A multiobjective function is utilized to coordinate DCG and PSS by a modified DE and PSO control algorithm. Now governor provides mechanical damping torque and PSS provides electrical torque, so proper coordination between them is performed in the proposed control action. A time delay is incorporated with a speed deviation signal for the governor system as it is a remote signal. Equation (38) presents state-space model of PSHPP with the proposed controller. The elements of matrix [A] are given in the appendix.

$$\Delta \dot{X} = A\Delta X, \tag{38}$$

where $\Delta \dot{X} = \begin{bmatrix} \Delta\dot{\delta}\Delta\dot{\omega}\Delta\dot{E}_q' \Delta\dot{E}_{\mathrm{fd}}\Delta\dot{V}_1 \ \Delta\dot{V}_{\mathrm{pss}} \ \Delta\dot{P}_m\Delta\dot{Y}\Delta\dot{Y}_1 \\ \Delta\dot{Y}_2\Delta\dot{X}_1 \ \Delta\dot{X}_2 \ \Delta\dot{C}_1\Delta\dot{C}_2\Delta\dot{C}_3\Delta\dot{U}_1\Delta\dot{U}_2 \end{bmatrix}$.

4. Multiobjective Function and Optimization Technique

4.1. Multiobjective Function. A multiobjective function in the time domain has been implemented here to damp system oscillations by minimizing speed and real power variation, overshoot, undershoot, and settling time simultaneously. The objective of the proposed work is to damp power system oscillations, for which two different objectives J_1 and J_2 are considered here. The objective J_1 is of ITAE type to damp variations is speed and real power as shown by equation (39). For multimachine systems, $\Delta\omega_e$ and ΔP_e are sum of speed and real power variations of all generators. The range of gain values K_{ps},Kw, K_{pe} are taken from 0 to 100. PID parameters K_p, K_i, and K_d gain values range from 0 to 50, 0–2, and 0–5, respectively. The range of time constants T_1, T_2, T_{e1}, T_{e2}, T_{p1}, and T_{p2} are taken from 0 to 1.

$$J_1 = \int_0^{t\,\mathrm{sim}} t\left|\Delta\omega_e\right|dt + \int_0^{t\,\mathrm{sim}} t\left|\Delta P_e\right|dt. \tag{39}$$

For objective function J_2 the system response characteristics such as undershoot (US), overshoot (OS), and settling time (T_{se}) have been considered with the same constraints as for J_1. Equation (40) shows function J_2, where normalized values of 4000 and 1000 are taken for US and OS, respectively.

$$J_2 = (4000 \times US)^2 + (1000 \times OS)^2 + T_{\mathrm{se}}^2. \tag{40}$$

The multiobjective function J_3 represented by equation (41) combines both J_1 and J_2 through weighing factor w_1 and w_2 and both are taken 0.5 in this study.

$$J_3 = (w_1 \times J_1) + (w_2 \times J_2). \tag{41}$$

4.2. Modified DE Algorithm. Differential evolution technique mainly depends upon the mutation strategies and control parameters, scaling factor (F), crossover rate (CR), Population (NP), and generation (G). For convergence in the modified differential evolution technique, F and CR are selected by the following expressions [36]:

$$F_G = F_{\max} e^{-a_1 G/G_{\max}}, \tag{42}$$

$$CR_G = CR_{\max} e^{-a_2 G/G_{\max}}. \tag{43}$$

Initially $G = 0$ which gives $F_{\mathrm{G}} = F_{\mathrm{MAX}}$ and $\mathrm{CR}_G = \mathrm{CR}_{\mathrm{MAX}}$ and in last generation when $G = G_{\mathrm{MAX}}$, $F_{\mathrm{G}} = F_{\mathrm{MIN}}$ and $\mathrm{CR}_G = \mathrm{CR}_{\mathrm{MIN}}$, where F_G and CR_{G} = Generation value of F and CR. F_{MAX} and F_{MIN} = maximum and minimum values of F, which are taken as 1 and 0, respectively. $\mathrm{CR}_{\mathrm{MAX}}$ and $\mathrm{CR}_{\mathrm{MIN}}$ = maximum and minimum values of CR, which are taken as 1 and 0, respectively. a_1 and a_2 = constants taken as 0.5 & 0.6, respectively.

4.3. PSO Algorithm. Velocity and position of swarms are the two main parameters of particle swarm optimization in a particular area. Equations (44) and (45) represent the velocity and the position of swarms, where acceleration coefficients and inertia weight are c_1, c_2, and w, respectively, whose limits are between 0.4 to 0.9. Two random values are rand_1 and rand_2, whose range is (0-1). Equation (45) represents the next iteration for the best solution.

$$v_i^{k+1} = \mathrm{wv}_i^k + c_1\,\mathrm{rand}_1\left(P_{i,p\,\mathrm{best}}^k - x_i^k\right) + c_2\,\mathrm{rand}_2\left(P_{i,g\,\mathrm{best}}^k - x_i^k\right), \tag{44}$$

$$x_i^{new} = x_i + v_i, \tag{45}$$

$$x_i^{k+1} = \begin{cases} x_{i,\mathrm{new}} if f\left(x_{i,\mathrm{new}}\right) \le f\left(x_i\right) \\ x_i \mathrm{otherwise} \end{cases}. \tag{46}$$

4.4. Proposed Hybrid MDEPSO Algorithm. MDE has the advantage over DE that it can choose suitable F and CR at the time of the program run, which exponentially decays from 1 to 0.01 and speeds up the computational time. Due to lack of storage in MDE, the result may be local optima, which is the demerit of MDE. PSO provides the global best value and can be easily implemented. Hence hybrid MDEPSO optimization technique has been developed considering the advantages of both MDE and PSO. The pseudocode of MDEPSO is presented in the following subsection and minimizations with different benchmarks taken from [39] as presented in Figure 7 are shown in Figure 8. Minimization data with different benchmarks are depicted in Table 1.

Pseudocode of MDEPSO:

(a) $X_1$are the initialized random particle.

(b) Generation starts at $G = 0$.

(c) Evaluate Fit_1 by using equation (41).

(d) MDE algorithm starts

(i) Calculation of F_G and CR_G by using equations (42) and (43).

(ii) Construct the mutant vector X_2 by performing mutation and crossover.

(iii) Evaluate Fit_2 by using equation (41).

(e) PSO algorithm starts.

(i) Present population is X_2.

(ii) If Fit_1 > Fit_2 then Pbest is X_1 otherwise X_2.

(iii) Gbest is evaluated from all the best values.

(iv) By using equations (44) and (45), a new velocity and a new position X_3 are updated.

(v) Evaluate Fit_3 by using equation (41).

(vi) Best particle for the next generation is by comparing Fit_1, Fit_2, and Fit_3.
$X_{G+1} = X_1$ if Fit_1 is greater.
$= X_2$ if Fit_2 is greater.
$= X_3$ if Fit_3 is greater.

(vii) Generation $G = G+1$

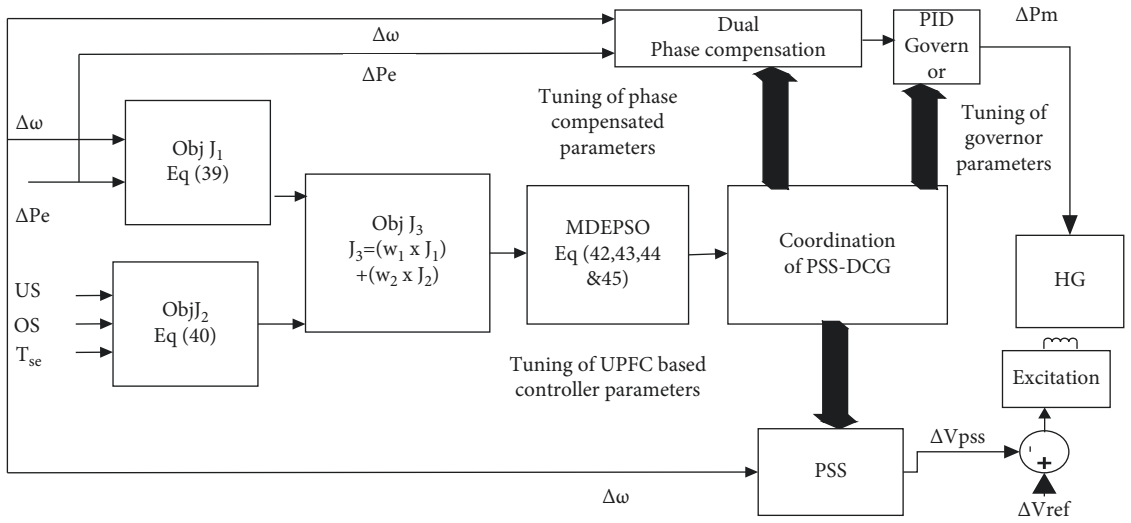

Figure 6: Strategy of proposed control action.

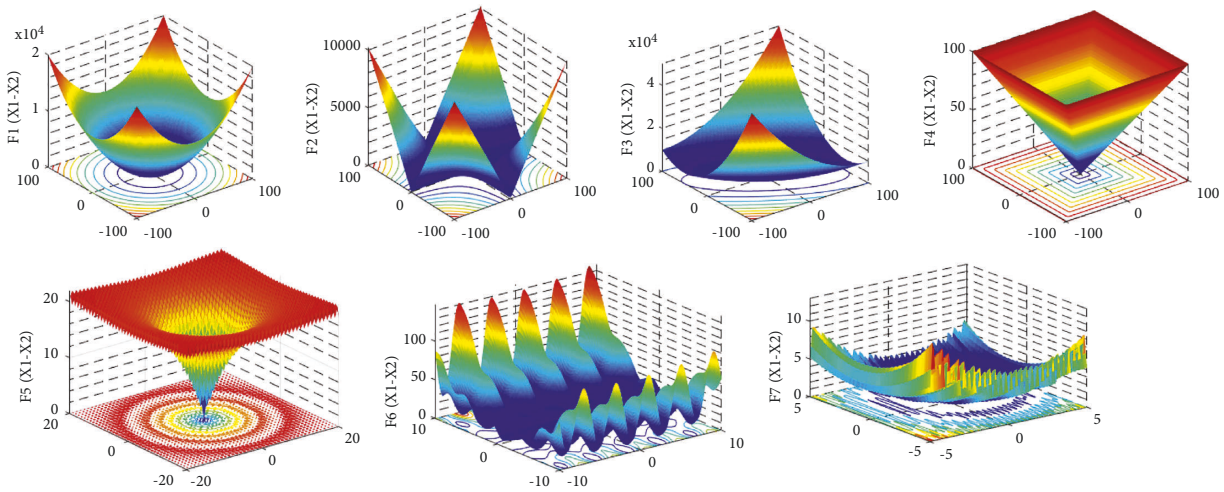

Figure 7: Representation of benchmarks.

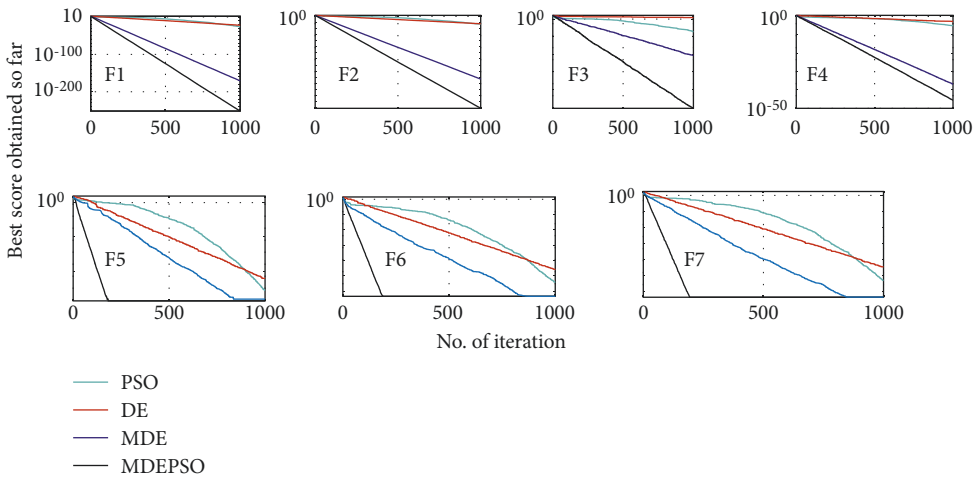

Figure 8: Representation of minimizations with benchmarks.

Table 1: Minimization data with different benchmarks.

Test function	Method	Best	Worst	Mean	Median	Std	Mode
$F_1(x) = \sum_{i=1}^{n} x_i^2$	DE	7.7076×10^{-23}	89.6814	1.8284	2.0515×10^{-10}	9.1087	2.5660×10^{-24}
	PSO	8.6825×10^{-26}	59.0523	0.3715	3.2881×10^{-05}	2.2602	0.8170
	MDE	1.5296×10^{-171}	97.0458	0.2873	4.6855×10^{-85}	3.9592	1.5296×10^{-171}
	MDEPSO	2.3716×10^{-252}	79.5738	0.1752	1.5736×10^{-125}	2.9696	5.6962×10^{-207}
$F_2(x) = \sum_{i=1}^{n} \lvert x_i \rvert + \prod_{i=1}^{n} \lvert x_i \rvert$	DE	7.5011×10^{-13}	37.4582	1.0757	5.5487×10^{-6}	4.3643	4.5889
	PSO	1.8587×10^{-13}	29.1477	0.6361	0.0054	1.6966	2.1191
	MDE	7.1634×10^{-104}	44.3117	0.1833	1.1278×10^{-51}	2.1493	7.1634×10^{-104}
	MDEPSO	7.6077×10^{-152}	32.7141	0.1087	6.6201×10^{-76}	1.4545	1.2815×10^{-79}
$F_3(x) = \sum_{i=1}^{n} (\sum_{j=1}^{i} x_j)^2$	DE	7.4006	122.8660	19.4567	17.7388	14.8076	9.3429
	PSO	1.2930×10^{-7}	100.0919	0.9153	0.0903	3.9796	1.8530
	MDE	2.1968×10^{-21}	131.55	1.4566	3.6139×10^{-10}	8.5265	1.7430×10^{-18}
	MDEPSO	1.9980×10^{-51}	113.8315	0.9322	5.3824×10^{-25}	6.9157	1.9269×10^{-42}
$F_4(x) = \max\{\lvert x_i \rvert, 1 \le i \le x\}$	DE	0.0028	4.1333	0.5414	0.1241	0.8711	0.0053
	PSO	6.6978×10^{-08}	9.4554	0.9784	0.0864	3.9756	1.5098
	MDE	1.6120×10^{-37}	4.3952	0.0493	1.0167×10^{-18}	0.3291	9.9964×10^{-23}
	MDEPSO	2.6549×10^{-46}	3.4157	0.0331	5.0452×10^{-23}	0.2459	1.3978×10^{-21}
$F_5(x) = -20\ \exp(-0.2\sqrt{\frac{1}{n}\sum_{i=1}^{n} x_i^2})$	DE	8.3391×10^{-12}	8.4747	0.4290	1.0178×10^{-5}	1.3745	2.5207×10^{-6}
$-\exp(\frac{1}{n}\sum_{i=1}^{n} \cos\ 2\ \pi x_i) + 20 + e$	PSO	1.4655×10^{-13}	7.3576	0.4471	0.0046	0.8084	0.9592
	MDE	7.9936×10^{-15}	9.1044	0.1612	8.1599×10^{-9}	0.6809	7.9936×10^{-15}
	MDEPSO	4.4409×10^{-15}	8.0835	0.0657	4.4409×10^{-15}	0.5884	4.4409×10^{-15}
$F_6(x) = \prod_{n} \left[\begin{array}{c} 10\sin^2(\prod y_i) + \\ \sum_{i=1}^{n} (y_i - 1)^2 [1 + 10\ \sin^2(3\prod y_i + 1)] \\ + \sum_{i=1}^{n} u(x_i, 10, 100, 4) \end{array} \right]$	DE	1.0362×10^{-23}	4.9303	0.1010	9.6834×10^{-12}	0.4991	0.0086
	PSO	8.7535×10^{-28}	3.8336	0.0155	1.5919×10^{-7}	0.1563	0.0099
	MDE	2.4163×10^{-32}	5.6529	0.0116	3.8120×10^{-20}	0.1566	2.4163×10^{-32}
	MDEPSO	2.3558×10^{-32}	3.3128	0.0176	2.3558×10^{-32}	0.2426	2.3558×10^{-32}
$F_7(x) = 0.1 \left[\begin{array}{c} \sin^2(3\prod x_i) + \\ \sum_{i=1}^{n} (x_i - 1)^2 [1 + \sin^2(3\prod x_i + 1)] \\ + (x_n - 1)^2 [1 + \sin^2(2\prod x_n)] \\ + \sum_{i=1}^{n} u(x_i, 8, 100, 4) \end{array} \right]$	DE	4.2714×10^{-23}	12.3192	0.2460	2.9953×10^{-11}	1.2454	1.3498×10^{-32}
	PSO	2.1554×10^{-27}	8.1581	0.0596	3.5052×10^{-6}	0.3416	0.1303
	MDE	1.4730×10^{-32}	16.5653	0.0530	1.0710×10^{-20}	0.4652	1.4730×10^{-32}
	MDEPSO	1.3498×10^{-32}	9.0389	0.0633	1.3498×10^{-32}	0.8376	1.3498×10^{-32}

(viii) Maximum generation is checked. If no, then repeat again from step (*C*).

5. Case Studies and Analysis

In this work, the electromechanical oscillations are to be damped by the proposed control action. So, different cases are experimented with to justify the controller objective. A four-machine, two-area, and 39-bus new England system is considered for study. The system data is presented in Table 2. At first, the governor performance was compared with dual compensated governor and the coordinated DCG-PSS actions are observed with different operating conditions of hydro generators are considered equipped with DCG and PSS. MDEPSO algorithm is employed to tune controller parameters with multiobjective function J_3.

5.1. Case-I. Performance Analysis of Dual Compensated Governor. Here a two-area system with four hydro generators is considered with sudden penetration of SPV and wind sources. The system is shown in Figure 9 and the initial operating state of hydro generators is in Table 3. With this operating condition, three different conditions are executed with sudden SPV and wind variations. In condition-I, SPV output is raised suddenly to 0.5 pu, in condition-II, wind output is suddenly raised to 0.5 pu, and in condition-III, both SPV and wind output are raised suddenly to 0.3 pu and 0.7 pu, respectively. The system response comparisons for DCG and uncompensated governors are presented in Figures 10 and 11, subject to local oscillations of all generators.

Table 4 presents optimal parameters for all generators for different conditions. The system response predicts that DCG provides a better response as compared to only governor action to damp oscillations.

5.2. Case-II. Sudden Variation in SPV and Wind Penetration

5.2.1. Time and Frequency Domain Analysis. In this case, sudden SPV and wind penetration are executed subject to different operating conditions. A two-area four hydro generator system is shown in Figure 9 and has been taken for this case. The initial operating state of all generators is given in Table 1. With these generators, sudden SPV and wind penetration are executed at Bus-1 to Bus-4 at different instants. The SPV and wind penetrations are suddenly raised by 0.3 pu and 0.7 pu, respectively. The local oscillations for all generators are examined independently with only PSS, Gov-PSS, Single compensated governor with PSS (CG-PSS), and proposed dual compensated governor with PSS (DCG-PSS) tuned by DE, PSO, and multiobjective MDEPSO algorithms. The local oscillations for G_1 and G_2 are shown in Figure 12, for G_3 and G_4 are shown in Figure 13, and interarea oscillations are shown in Figure 14. Figure 15 depicts settling time comparisons with different control actions. These interarea oscillations are observed when sudden SPV and wind penetrations are applied to machine-1, machine-2, machine-3, and machine-4 separately and presented for ω_{14}, ω_{23},ω_{32}, and ω_{41}, respectively. Tables 5 and 6 present mechanical oscillatory mode and optimized gains, respectively. In Table 5, the oscillatory mode with governor and excitation system as reported in [37] has also been compared with the proposed control action, and the eigenvalues are found to move towards a more stable region with the proposed control action. In [37], the governor and excitation control action has been implemented for a single machine system, but in this work, this action has been implemented for all four generators separately for analysis purposes. Stability analysis in the frequency domain has also been performed in this case, subject to simultaneous solar and wind penetration. For this analysis, Bode plots have been performed and Table 7 represents the Bode plot for local oscillations of all the generators. The positive gain margin and phase margin in the Bode plots signify the stability of the system with the proposed control action. The higher synchronous generation contribution led to a better stability region in frequency analysis via Bode plots. It is found that oscillations are more excited with fewer generator output contributions. Oscillations are damped heavily with a higher operating state of generators with more active power contributions. Also, dual compensation of the governor in coordination with PSS can provide efficient damping to these oscillations, which has been justified by system oscillatory responses.

5.2.2. Sensitivity Analysis for Parametric Variations. The robustness of the system with the proposed control action can be analyzed with different uncertainties occurring in a practical power system. Besides changes in system operating conditions and variation in renewable power generation, as considered earlier, the parametric variation has been considered in this section. Sensitivity analysis has been performed in this case subject to variation in excitation system, governor, and prime mover parameters considering G1 in a multimachine system as shown in Figure 9. The system local eigenvalues, settling time, and minimum damping ratios are presented in Table 8. In this case, the excitation system

Table 2: System data.

Hydro generator	Rated = 100 MVA, rated turbine o/p = 90.94 MW, turbine discharge rate = 71.43 m^3/s, turbine head = 138.9 m, gate position = 0.9 pu, discharge without load = 4.3 m^3/s, permanent droop R_p = 0.05 pu, pilot time constant = 0.02 s, servo time constant = 0.5 s, penstock length = 465 m and cross-sectional area = 15.2 m^2
SPV and wind generation	$K_{WG} = 1.0$, $T_{WG} = 1.5$, $K_V = 1.0$, $T_V = 1.8$
Trans line	$V_{nominal} = 230$ kV, $L1 = 25$ km, $L2 = 10$ km, $L3 = 110$ km $R = 1.0 \times 10^{-4}$ pu/km, XL = 1.0×10^{-3} pu/km, BC = 1.75×10^{-3} pu/km

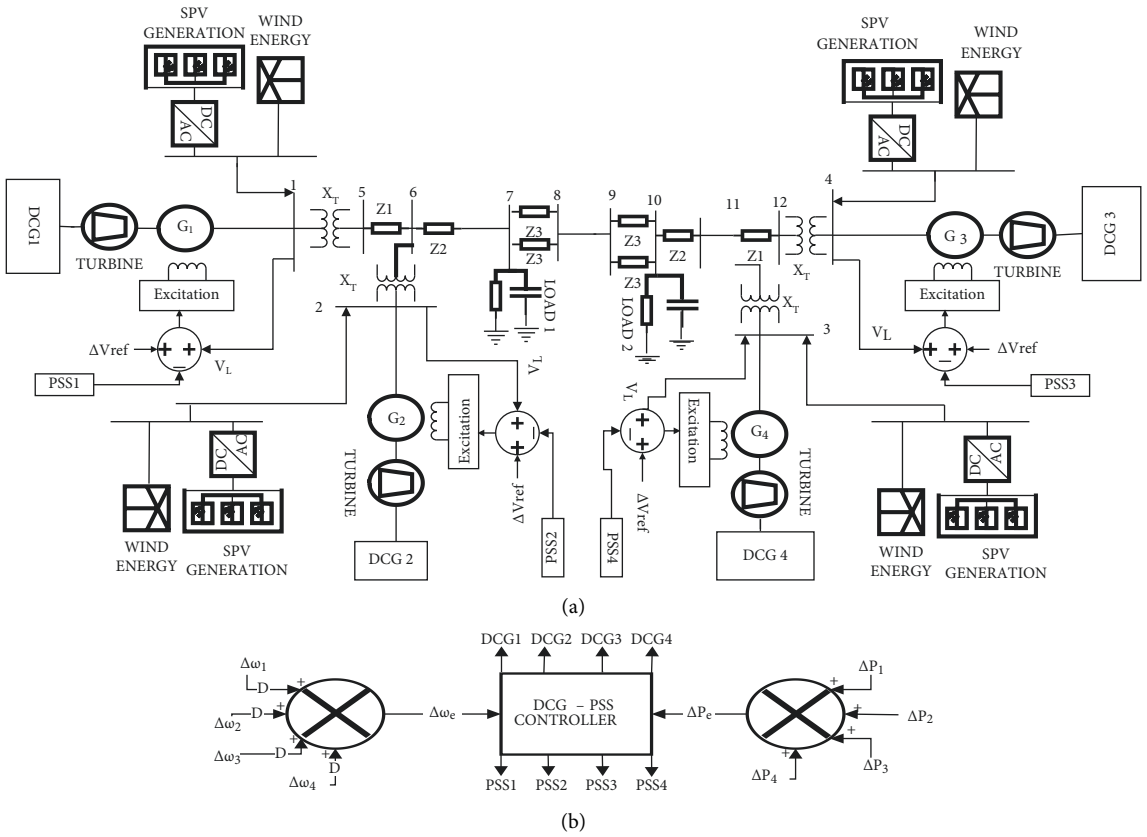

Figure 9: (a) Two area system under study. (b) Control unit block.

Table 3: Initial operating condition for hydro generators for four m/c system.

Real (P_0)/reactive power (Q_0)	$G1$	$G2$	$G3$	$G4$
P_0 (pu)	0.9	0.6	0.8	0.71
Q_0 (pu)	0.12	0.25	0.17	0.20

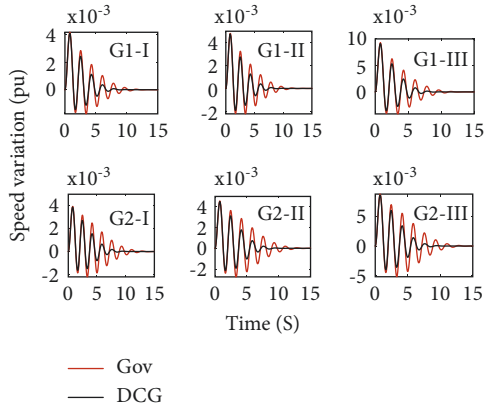

Figure 10: Angular frequency variation for G_1 and G_2.

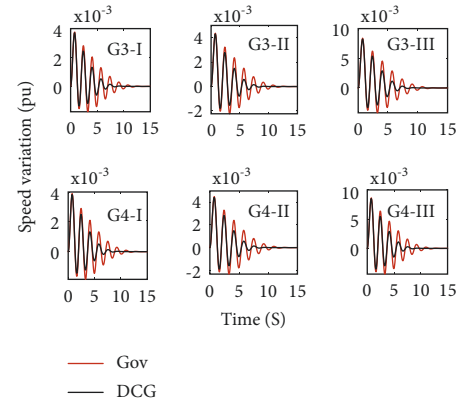

Figure 11: Angular frequency variation for G_3 and G_4.

Table 4: Optimal parameters.

Parameters	SPV output raised by 0.5 pu		Wind output raised by 0.5 pu		SPV output raised by 0.3 pu with wind output raised by 0.7 pu simultaneously	
	CGov	Gov	CGov	Gov	CGov	Gov
K_{p1}	33.872	43.116	8.973	36.35	41.85	17.67
K_{p2}	37.476	25.685	10.273	42.58	7.87	25.47
K_{p3}	17.071	35.447	14.465	39.61	15.81	40.88
K_{p4}	25.171	17.851	37.267	28.56	19.23	1.91
K_{i1}	1.632	0.323	0.492	1.34	1.31	0.904
K_{i2}	1.615	1.318	1.598	1.41	1.34	1.67
K_{i3}	1.291	0.514	0.922	0.579	0.562	0.281
K_{i4}	0.262	1.373	0.522	1.11	1.84	1.11
K_{d1}	4.871	3.638	4.235	4.31	2.56	3.45
K_{d2}	2.434	1.698	4.644	3.74	2.27	1.29
K_{d3}	4.518	3.388	3.954	2.96	2.95	1.15
K_{d4}	2.951	4.533	2.351	4.87	1.67	38.767
Kw_1	93.684	---	37.821	---	7.23	---
Kw_2	74.798	---	76.046	---	86.51	---
Kw_3	45.984	---	93.696	---	68.16	---
Kw_4	62.819	---	44.671	---	65.44	---
K_{pe1}	9.896	---	90.787	---	94.31	---
K_{pe2}	43.763	---	62.061	---	71.34	---
K_{pe3}	51.271	---	22.152	---	25.48	---
K_{pe4}	22.092	---	73.416	---	48.92	---
T_{e1}	0.739	---	0.728	---	0.703	---
T_{e2}	0.197	---	0.195	---	0.375	---
T_{e3}	0.119	---	0.341	---	0.774	---
T_{e4}	0.816	---	0.642	---	0.568	---
T_{e5}	0.531	---	0.257	---	0.245	---
T_{e6}	0.697	---	0.637	---	0.248	---
T_{e7}	0.606	---	0.132	---	0.655	---
T_{e8}	0.259	---	0.847	---	0.598	---
T_{p1}	0.921	---	0.668	---	0.687	---
T_{p2}	0.491	---	0.435	---	0.394	---
T_{p3}	0.781	---	0.607	---	0.952	---
T_{p4}	0.504	---	0.335	---	0.445	---
T_{p5}	0.677	---	0.359	---	0.782	---
T_{p6}	0.159	---	0.638	---	0.404	---
T_{p7}	0.845	---	0.268	---	0.803	---
T_{p8}	0.208	---	0.262	---	0.866	---

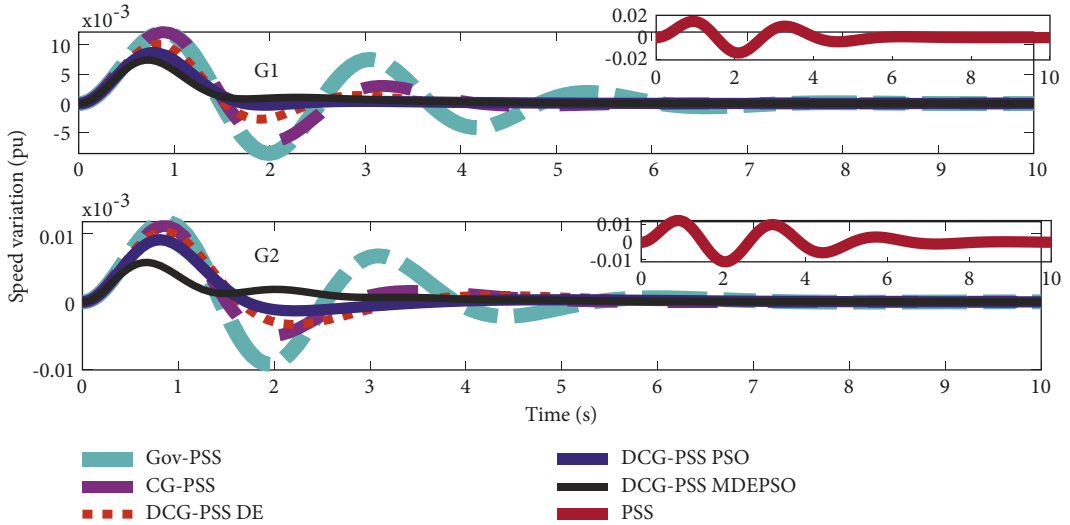

Figure 12: Angular frequency variation for G_1 and G_2.

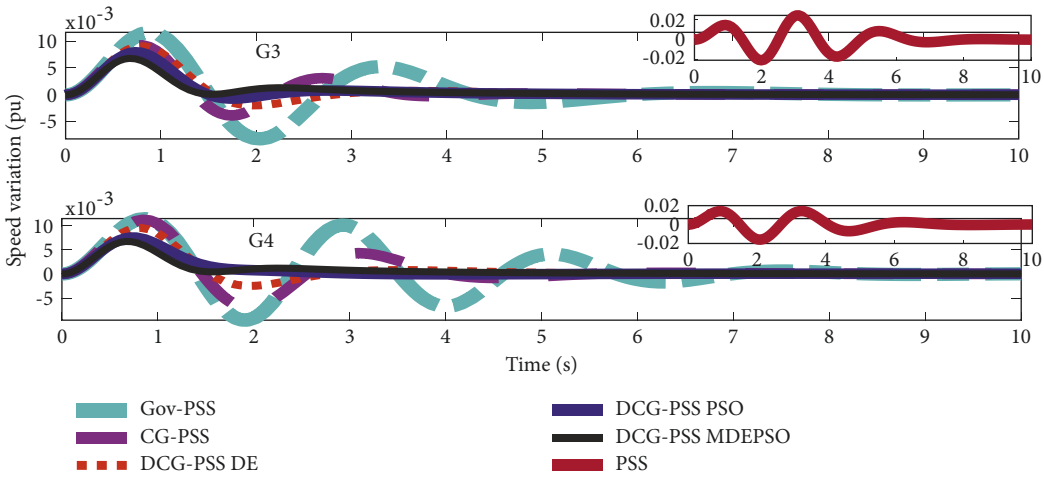

Figure 13: Angular frequency variation for G_3 and G_4.

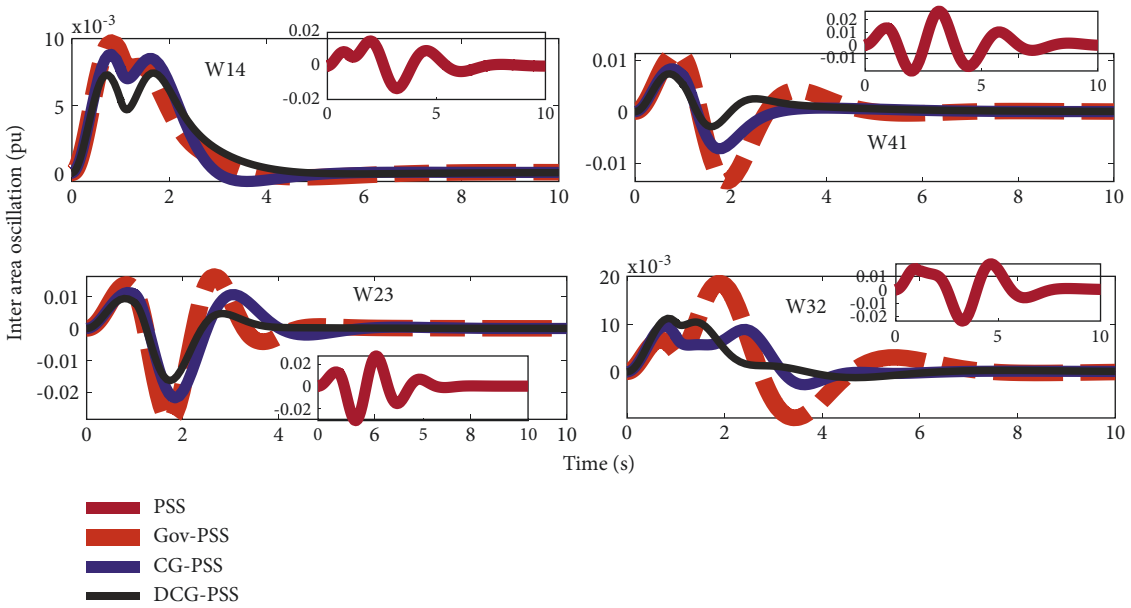

Figure 14: Inter-area oscillation of ω_{14}, ω_{41}, ω_{23} and ω_{32}.

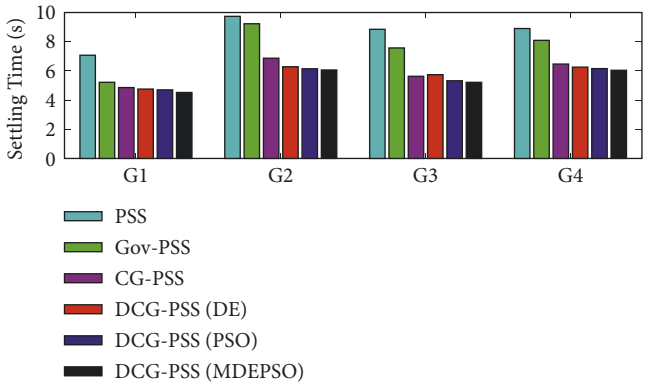

Figure 15: Settling time comparisons with different control actions.

Table 5: Mechanical mode for local oscillations.

System	PSS	Gov-PSS [37]	Coordinated Gov-PSS	Coordinated CG-PSS	Proposed coordinated DCG-PSS
G1	$-3.9265 + 4.6293i$	$-1.9265 + 7.6296i$	$-3.9426 + 4.6197i$	$-4.0322 + 4.6055i$	$-3.9324 + 4.6244i$
	$-3.9265 - 4.6293i$	$-1.9265 - 7.6296$i	$-3.9426 - 4.6197i$	$-4.0322 - 4.6055i$	$-3.9324 - 4.6244i$
	$-0.6168 + 3.0837i$	$-0.0668 + 3.0131i$	$-0.0853 + 3.2578i$	$-0.0671 + 3.6037i$	$-1.808 + 3.2894i$
	$-0.6168 - 3.0837i$	$-0.0668 - 3.0131i$	$-0.0853 - 3.2578i$	$-0.0671 - 3.6037i$	$-1.808 - 3.2894i$
G2	$-3.9370 + 4.6245i$	$-1.9371 + 9.8871$i	$-3.9614 + 4.6290i$	$-3.9666 + 4.6666i$	$-3.9729 + 4.6247i$
	$-3.9370 - 4.6245i$	$-1.9371 - 9.8871$i	$-3.9614 - 4.6290i$	$-3.9666 - 4.6666i$	$-3.9729 - 4.6247i$
	$-1.0144 + 2.0551i$	$-0.0132 + 2.0523$i	$-1.3807 + 2.3670i$	$-0.0913 + 3.6233i$	$-1.2890 + 2.9189i$
	$-1.0144 - 2.0551i$	$-0.0132 - 2.0523$i	$-1.3807 - 2.3670i$	$-0.0913 - 3.6233i$	$-1.2890 - 2.9189i$
G3	$-3.9744 + 4.6789i$	$-1.9751 + 7.6661$i	$-4.0268 + 4.7275i$	$-3.9674 + 4.6382i$	$-4.0947 + 4.7168i$
	$-3.9744 - 4.6789i$	$-1.9751 - 7.6661$i	$-4.0268 - 4.7275i$	$-3.9674 - 4.6382i$	$-4.0947 - 4.7168i$
	$-0.5998 + 2.7791i$	$-0.0991 + 4.2111$i	$-0.1806 + 3.6584i$	$-0.5016 + 3.0458i$	$-1.4459 + 2.5127i$
	$-0.5998 - 2.7791i$	$-0.0991 - 4.2111i$	$-0.1806 - 3.6584i$	$-0.5016 - 3.0458i$	$-1.4459 - 2.5127I$
G4	$-4.0207 + 4.6712i$	$-1.0727 + 8.6712i$	$-3.9548 + 4.5862i$	$-3.9464 + 4.6296i$	$-3.9508 + 4.6214i$
	$-4.0207 - 4.6712i$	$-1.0727 - 8.6712i$	$-3.9548 - 4.5862i$	$-3.9464 - 4.6296i$	$-3.9508 - 4.6214i$
	$-0.2019 + 3.2541i$	$-0.2028 + 3.2577i$	$-0.0611 + 3.2038i$	$-0.0011 + 3.6178i$	$-1.3135 + 3.1889i$
	$-0.2019 - 3.254i$	$-0.2028 - 3.2577i$	$-0.0611 - 3.2038i$	$-0.0011 - 3.6178i$	$-1.3135 - 3.1889i$

Table 6: Optimized gains.

Parameters	PSS	Coordinated Gov-PSS	Coordinated CG-PSS	Coordinated DCG-PSS (DE)	Coordinated DCG-PSS (PSO)	Proposed coordinated DCG-PSS (MDEPSO)
K_{ps1}	70.68	96.55	73.17	81.54	51.85	40.68
K_{ps2}	56.73	89.67	58.45	48.33	65.22	17.47
K_{ps3}	71.43	91.93	39.98	85.09	31.48	54.32
K_{ps4}	54.48	76.62	68.29	92.37	90.96	70.00
T_1	0.879	0.336	0.324	0.901	0.481	0.269
T_2	0.666	0.211	0.286	0.657	0.311	0.676
T_3	0.462	0.472	0.601	0.771	0.627	0.231
T_4	0.307	0.299	0.678	0.846	0.927	0.492
T_5	0.633	0.216	0.824	0.281	0.642	0.657
T_6	0.361	0.337	0.841	0.461	0.838	0.986
T_7	0.647	0.793	0.788	0.123	0.101	0.167
T_8	0.721	0.608	0.858	0.932	0.629	0.777
K_{p1}	-------	7.638	41.02	30.86	32.11	17.33
K_{p2}	-------	8.815	35.51	36.01	22.05	13.24
K_{p3}	-------	13.05	23.29	33.62	11.37	15.87
K_{p4}	-------	46.04	38.16	37.81	26.20	44.72
k_{i1}	-------	1.596	1.542	1.051	1.374	1.087
K_{i2}	-------	0.171	0.026	0.081	0.697	1.197
K_{i3}	-------	1.171	1.613	1.359	0.327	0.901
K_{i4}	-------	0.594	1.696	1.384	0.728	1.296
k_{d1}	-------	3.011	4.585	2.946	2.154	1.063
K_{d2}	-------	3.755	1.996	3.354	3.488	4.452
K_{d3}	-------	1.527	3.343	1.098	2.675	3.015
K_{d4}	-------	2.491	1.754	2.727	4.831	3.731
Kw_1	-------	-------	49.31	66.36	88.80	33.28
Kw_2	-------	-------	91.19	55.12	17.34	68.06
Kw_3	-------	-------	75.24	11.12	6.521	90.05
Kw_4	-------	-------	19.50	75.93	58.07	99.91
T_{p1}	-------	-------	0.445	0.183	0.373	0.589
T_{p2}	-------	-------	0.184	0.555	0.791	0.123
T_{p3}	-------	-------	0.684	0.535	0.887	0.995
T_{p4}	-------	-------	0.543	0.358	0.617	0.432
T_{p5}	-------	-------	0.375	0.244	0.518	0.107
T_{p6}	-------	-------	0.641	0.515	0.737	0.515
T_{p7}	-------	-------	0.145	0.477	0.861	0.241
T_{p8}	-------	-------	0.541	0.107	0.206	0.438
K_{pe1}	-------	-------	-------	93.58	56.76	31.52
K_{pe2}	-------	-------	-------	58.41	34.83	70.68

Table 6: Continued.

Parameters	PSS	Coordinated Gov-PSS	Coordinated CG-PSS	Coordinated DCG-PSS (DE)	Coordinated DCG-PSS (PSO)	Proposed coordinated DCG-PSS (MDEPSO)
K_{pe3}	-------	-------	-------	86.03	52.77	90.90
K_{pe4}	-------	-------	-------	35.42	79.15	88.71
T_{e1}	-------	-------	-------	0.862	0.294	0.383
T_{e2}	-------	-------	-------	0.148	0.424	0.692
T_{e3}	-------	-------	-------	0.951	0.269	0.683
T_{e4}	-------	-------	-------	0.148	0.305	0.121
T_{e5}	-------	-------	-------	0.986	0.423	0.257
T_{e6}	-------	-------	-------	0.347	0.272	0.735
T_{e7}	-------	-------	-------	0.162	0.145	0.688
T_{e8}	-------	-------	-------	0.946	0.726	0.457

Table 7: Bode plot.

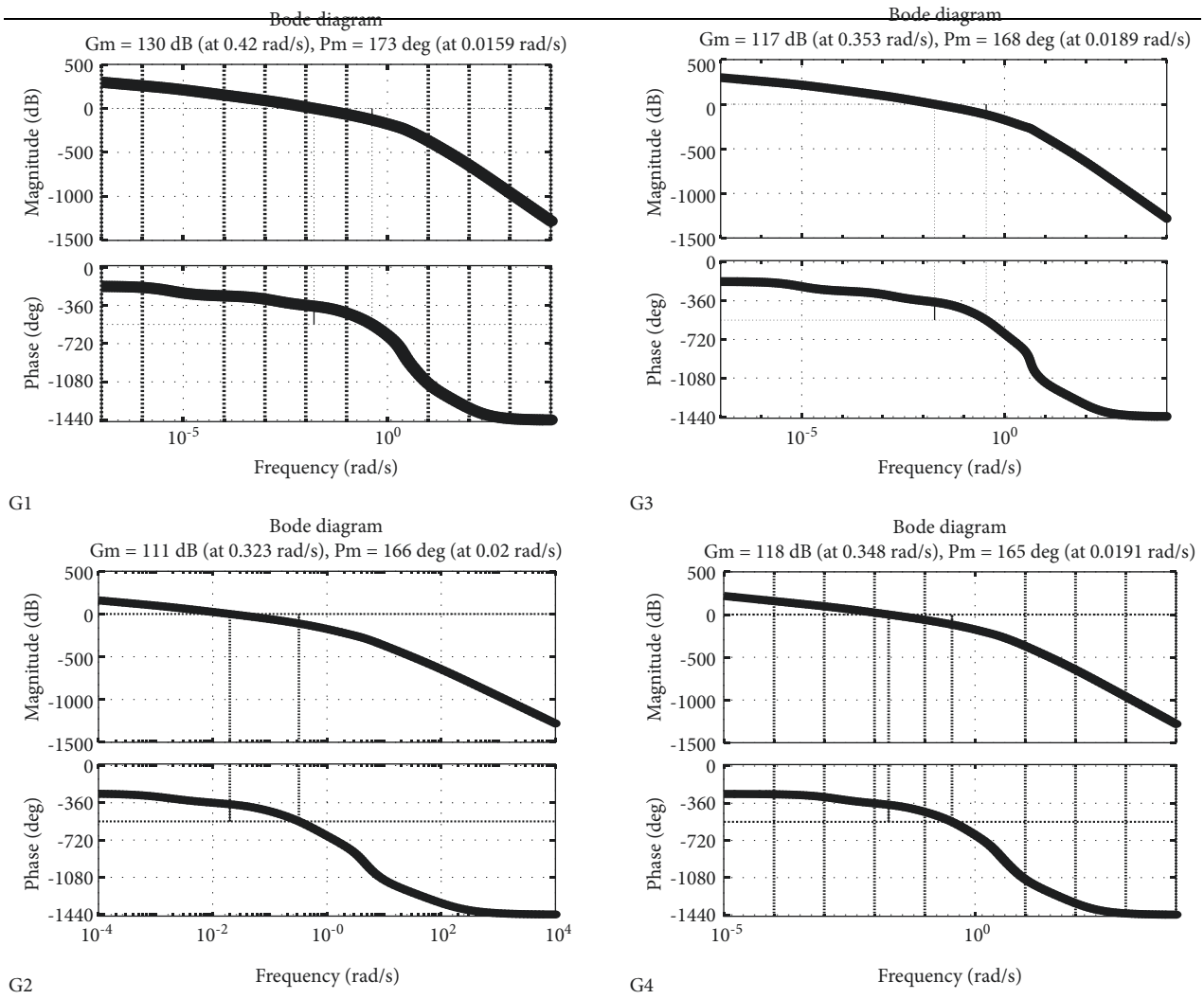

parameter T_a, the governor servo motor parameter T_c and prime mover water time constant T_{tw} are raised and lowered by 50%. From the system eigen-distribution, it is observed that subject to parametric variation, which may occur in a practical power system, all the eigenvalues have negative real part predicting stability of the system. So, with the proposed controller, the stability of the system can be justified pertaining to parameter variation, which signifies robustness of the control action. Also, the minimum damping ratio with less settling time within 5 s predicts that even though system

Table 8: Eigen distributions for parametric variations.

Parameter change	Eigen value	Settling time	Minimum damping ratio
T_a decreased by 50%	$1.0e+02*$ $-1.9965, -0.5000, -0.2733, -0.1969, -0.0007+0.0569i, -0.0007-0.0569i, -0.0434+0.0490i, -0.0434-0.0490i, -0.0332, -0.0278, -0.0180, -0.0015+0.0006i, -0.0015-0.0006i, -0.0009, -0.0010, -0.0067, -0.0056$	4.2258	0.0122
T_a raised by 50%	$-66.7194, -49.9829, -27.5268, -19.3836, -0.1002+6.4346i, -0.1002-6.4346i, -4.4724+5.0343i, -4.4724-5.0343i, -2.5694, -1.9417, -1.6843, -0.1474+0.0625i, -0.1474-0.0625i, -0.0901, -0.0017, -0.1000, -0.6667, -0.5556$	4.3302	0.0156
T_c decreased by 50%	$-99.7238, -50.0381, -31.0300, -19.1870, -7.5659+3.2935i, -7.5659-3.2935i, -0.0297+5.6774i, -0.0297-5.6774i, -1.4702, -1.9512, -1.9280, -0.1606+0.0442i, -0.1606-0.0442i, -0.0981, -0.0017, -0.1000, -0.6667, -0.5556$	4.5032	0.0522
T_c raised by 50%	$-99.7515, -50.0006, -26.4410, -19.7465, -0.1563+5.6422i, -0.1563-5.6422i, -3.0743+4.5920i, -3.0743-4.5920i, -1.7397, -1.7127, -1.6187, -0.1467+0.0616i, -0.1467-0.0616i, -0.0911, -0.0017, -0.1000, -0.6667, -0.5556$	4.4131	0.0277
T_{tw} decreased by 50%	$-99.7217, -50.0170, -27.1666, -19.8390, -0.1018+5.5947i, -0.1018-5.5947i, -4.1998+4.6267i, -4.1998-4.6267i, -2.5689, -1.9972, -1.4085, -0.1443+0.0628i, -0.1443-0.0628i, -0.0975, -0.0009, -0.1000, -0.6667, -0.5556$	4.6244	0.0182
T_{tw} raised by 50%	$-99.7296, -49.9994, -27.3071, -19.7186, -4.2943+4.8820i, -4.2943-4.8820i, -0.0408+5.4871i, -0.0408-5.4871i, -2.3378, -1.4841, -1.1960, -0.1705+0.0200i, -0.1705-0.0200i, -0.0926, -0.0025, -0.1000, -0.6667, -0.5556$	4.6996	0.00743

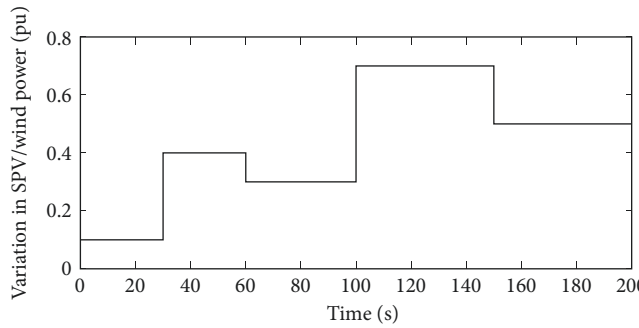

Figure 16: Pattern of solar/wind power variations.

parameters are largely varied, the system becomes stable within less time.

5.3. Case-III. Intermittent Variation in SPV and Wind Penetration. In this case, the four-machine system, as taken in the previous case and a modified new-England 39 bus system have been investigated for random SPV and wind penetrations penetrating to electromechanical oscillations. The pattern of this penetration is given in Figure 16. For a 4-machine system, this variation in SPV and wind generations have been applied independently and shown in Figures 17 and 18 for G_1, G_2, and G_3, G_4, respectively, for SPV variations. Similarly, Figures 19 and 20 for G_1, G_2, and G_3, G_4, respectively, for wind variations. The 39-bus system is being shown in Figure 21 with SPV and wind penetrations are executed at bus-6 and bus-25, respectively. The initial operating state of 10 machines is given in Table 9. These SPV and wind perturbations are executed separately at different timings. Figure 22 presents local oscillations for G_4, G_5, G_6, G_7, and interarea oscillations ω_{46}, ω_{58} when random SPV penetrations are executed at bus-6 and Figure 23 presents similar oscillations with random wind penetration is executed at bus-25. For this case, the proposed multiobjective coordinated dual compensated to damp oscillations. The effectiveness of the proposed controller is observed with oscillations for generators with different initial states subject to intermittent SPV and wind penetrations at bus-6 and bus-25. For the practical implementation of the proposed work,

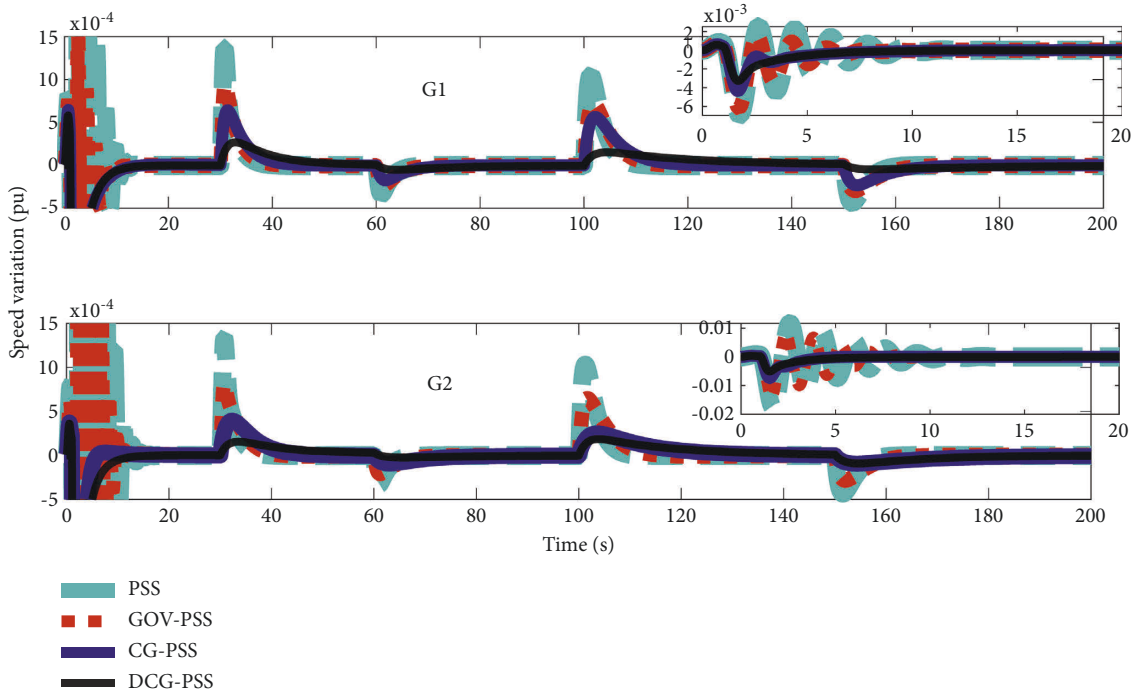

Figure 17: Speed variation for SPV change.

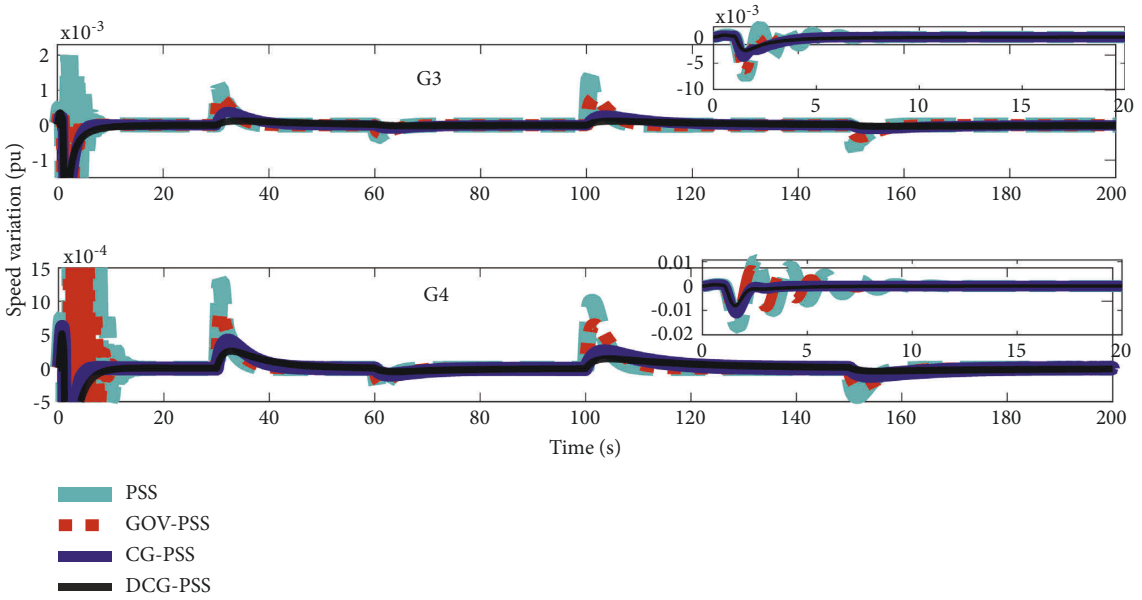

Figure 18: Speed variation for SPV change.

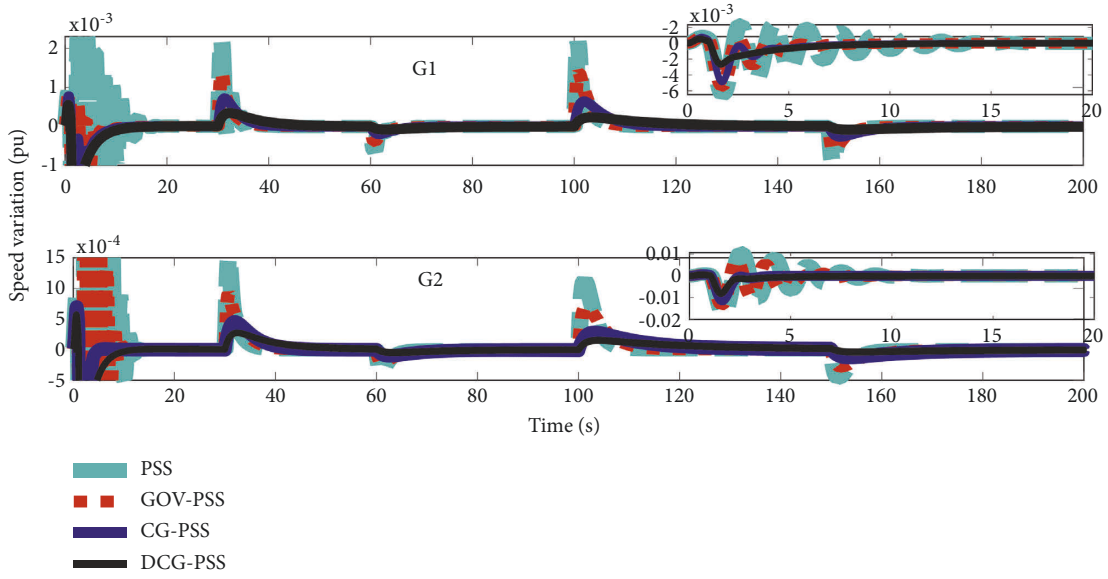

Figure 19: Speed variation for wind change.

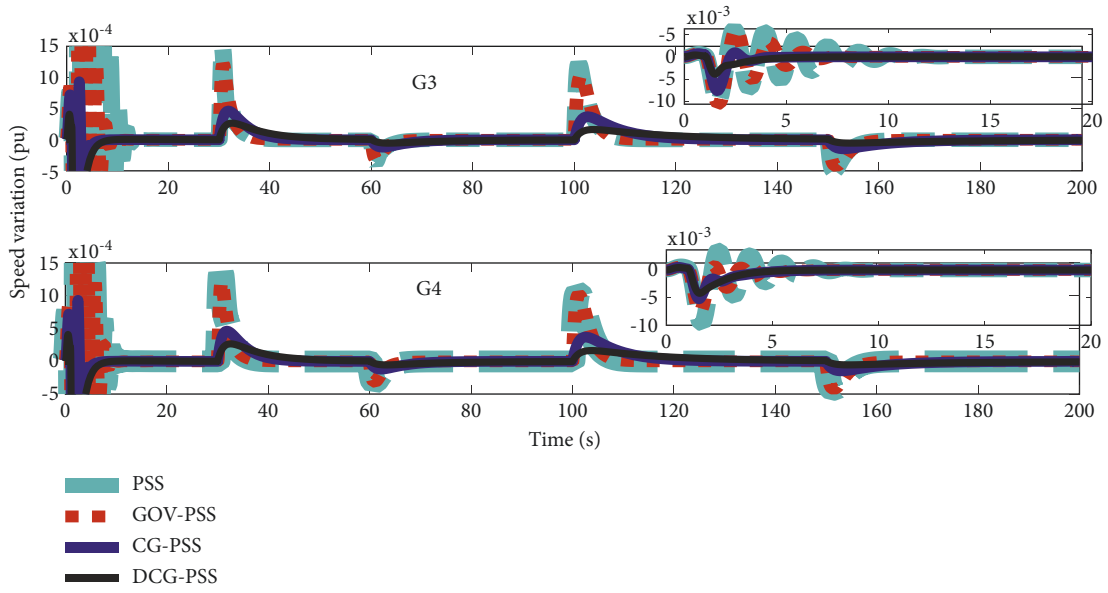

Figure 20: Speed variation for wind change.

the hardware control action and complexity of the model are mainly responsible. Also, there may be chances of instability during the running of the model for new parameters, and to tackle this, the flow of the MDEPSO algorithm can terminate simulation under this condition. Real time digital simulator (RTDS) can be implemented for testing the system in real-time. It is found from experimentations that intermittency in SPV and wind

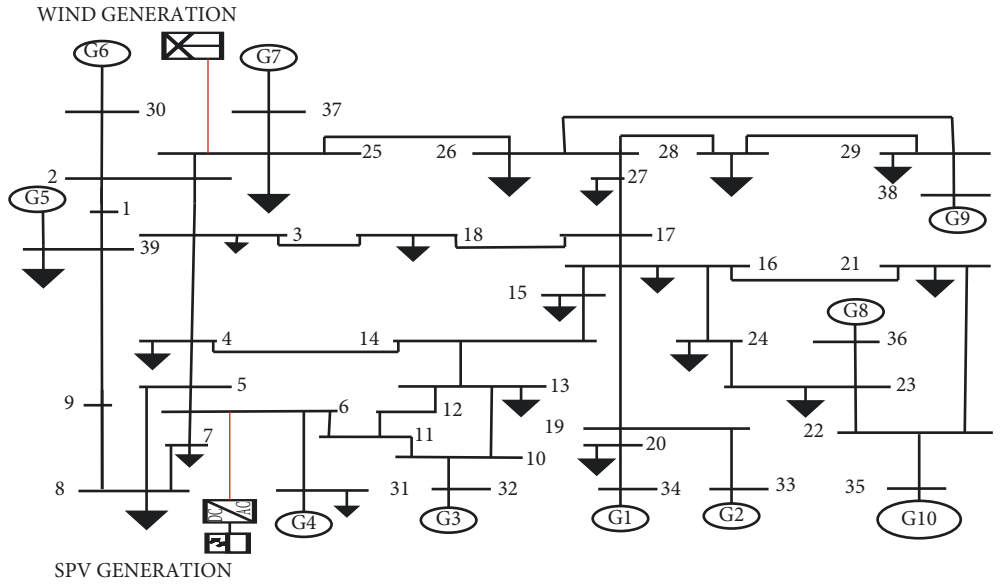

Figure 21: 39 bus system.

Table 9: Initial operating condition for hydro generators for 39 bus system.

Real power (P_0)/Reactive power (Q_0)	$G1$	$G2$	$G3$	$G4$	$G5$	$G6$	$G7$	$G8$	$G9$	$G10$
P_0 (pu)	0.71	0.8	0.6	0.9	0.8	0.6	0.71	0.9	0.6	0.8
Q_0 (pu)	0.20	0.17	0.25	0.12	0.17	0.25	0.20	0.12	0.25	0.17

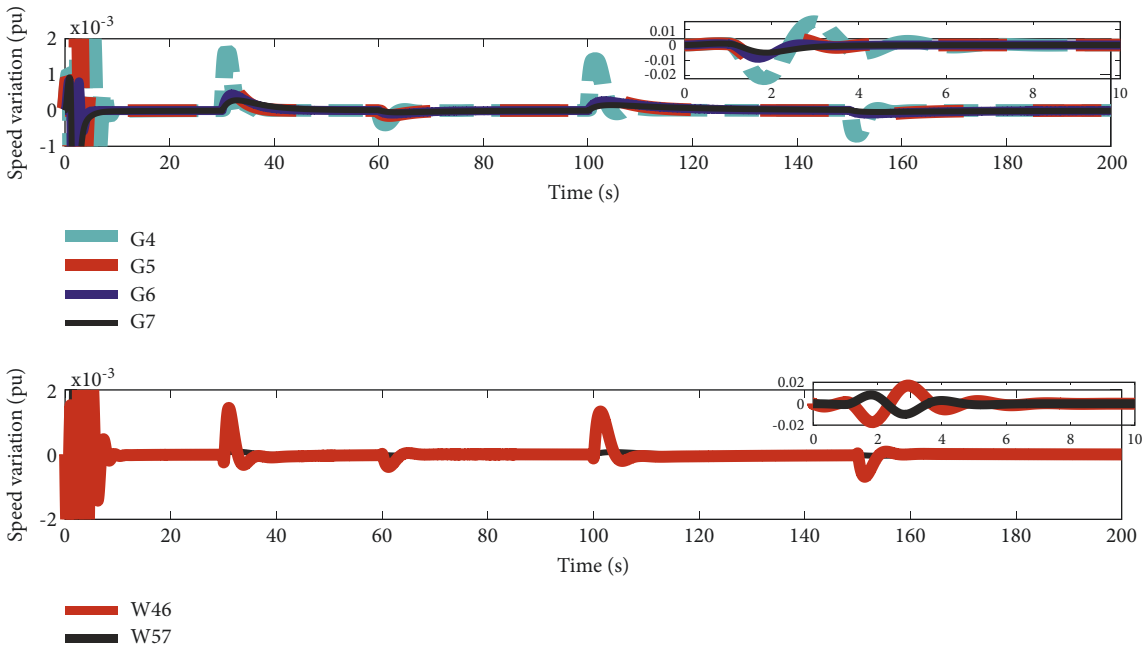

Figure 22: Angular frequency variation of G_4, G_5, G_6, and G_7.

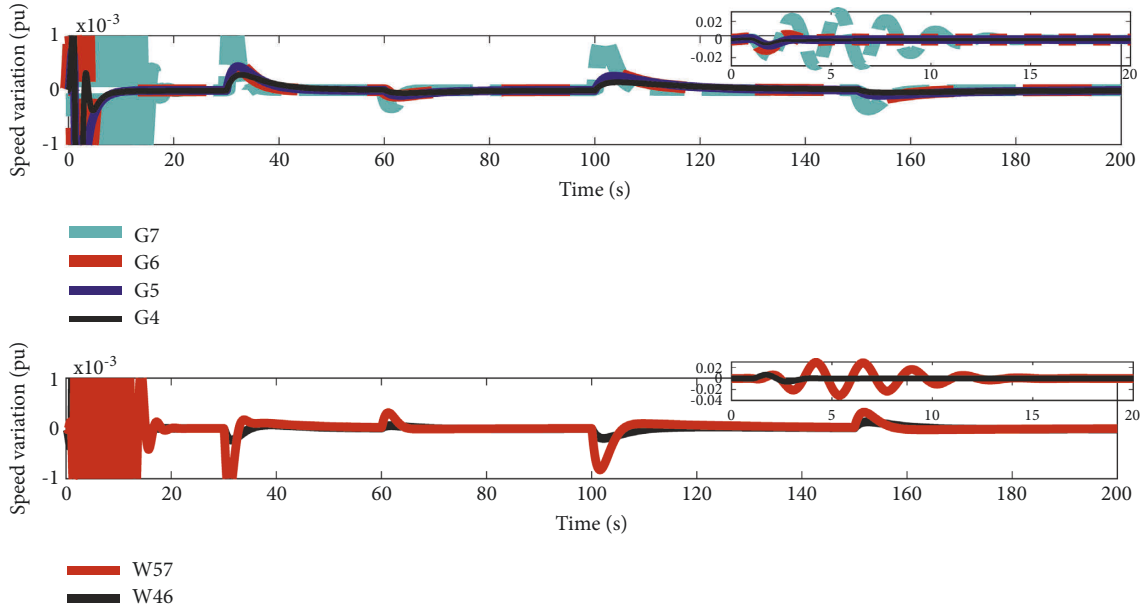

Figure 23: Angular frequency variation of G_4, G_5, G_6, and G_7.

penetration excites local and interarea oscillations and the proposed controller can efficiently dampen these oscillations.

6. Conclusion

The present work employed a coordinated damping control action of mechanical torque provided by hydro governor and electrical torque provided by PSS through excitation system by the help of a multiobjective function with a modified DE-PSO control algorithm for a hydro, wind, and SPV integrated power system. The experimentations with the findings of this study can be presented as follows:

(1) At first, the governor performances with dual compensation are compared with only conventional PID action, and the oscillations due to sudden SPV and wind variations are found to be damped better by additional dual phase lead incorporated with the governor.

(2) The PSS has been traditionally employed to damp oscillation, but when coordinated with a dual compensated governor (DCG), the damping capability is further enhanced. The multiobjective function employs minimization of speed and real power deviations, US, OS, and settling time for efficient damping action.

(3) The proposed control action is justified considering a four-machine two-area and 39-bus 10 m/c system as compared with conventional PID governor and PSS action. The local and remote signals, which are real power and speed deviations undergone through phase compensation and coordination of governor with PSS, are found to provide heavy damping action for critical oscillatory conditions.

(4) This work can be further extended to a large-scale extended power system with more renewable penetrations. For future work, multiple hydro governors with PSS can be optimally coordinated with time delay coordination to handle governor and excitation system dynamics.

Abbreviations

D:	Damping coefficient of generator
X_d', X_d:	Generator d-axis transient and steady state synchronous reactance
M:	Moment of inertia
K_V, T_V:	Gain and time constant of solar PV system
K_a, T_a:	Gain and time constant of AVR
K_{WG}, T_{WG}:	Gain and time constant of wind source
P_m, P_e:	Generator input mechanical power and output power
X_q:	Generator q-axis steady-state synchronous reactance
$\Delta\omega$, $\Delta\delta$:	Deviation in angular speed & deviation in rotor angle
K_c, T_c:	Gains and time constant of servo system-1
T_{d0}':	d-axis open circuit time constant
V_t:	Generator terminal voltage
R_P, D_t:	Permanent drop of governor and damping coefficient of turbine
K_{SM}:	Gain of governor
T_{tw}, t_a:	Time constant of water and servo system-2
Y:	Gate opening.

Appendix. A

Elements of matrix $[A]$:

$$A = \begin{vmatrix} o & A_{12} & 0 & 0 & 0 & 0 & 0 & 0 & 0 & 0 & 0 & 0 & 0 & 0 & 0 & 0 & 0 \\ A_{21} & A_{22} & A_{23} & 0 & 0 & 0 & A_{27} & 0 & 0 & 0 & 0 & 0 & 0 & 0 & 0 & 0 & 0 \\ A_{31} & 0 & A_{33} & A_{34} & 0 & 0 & 0 & 0 & 0 & 0 & 0 & 0 & 0 & 0 & 0 & 0 & 0 \\ A_{41} & 0 & A_{43} & A_{44} & 0 & A_{46} & 0 & 0 & 0 & 0 & 0 & 0 & 0 & 0 & 0 & 0 & 0 \\ A_{51} & A_{52} & A_{53} & 0 & A_{54} & 0 & A_{57} & 0 & 0 & 0 & 0 & 0 & 0 & 0 & 0 & 0 & 0 \\ A_{61} & A_{62} & A_{63} & 0 & A_{65} & A_{66} & A_{67} & 0 & 0 & 0 & 0 & 0 & 0 & 0 & 0 & 0 & 0 \\ A_{71} & A_{72} & A_{73} & 0 & 0 & 0 & A_{77} & A_{78} & A_{79} & 0 & 0 & 0 & 0 & 0 & 0 & 0 & 0 \\ 0 & 0 & 0 & 0 & 0 & 0 & 0 & A_{88} & A_{89} & 0 & 0 & 0 & 0 & 0 & 0 & 0 & 0 \\ 0 & 0 & 0 & 0 & 0 & 0 & 0 & 0 & 0 & A_{910} & 0 & 0 & 0 & 0 & 0 & 0 & 0 \\ 0 & 0 & 0 & 0 & 0 & 0 & 0 & A_{108} & 0 & A_{1010} & A_{1011} & A_{1012} & A_{1013} & 0 & 0 & A_{1016} & 0 \\ 0 & 0 & 0 & 0 & 0 & 0 & 0 & 0 & 0 & 0 & 0 & 0 & A_{1113} & 0 & 0 & A_{1116} & 0 \\ A_{121} & A_{122} & A_{123} & A_{124} & 0 & 0 & 0 & 0 & 0 & 0 & 0 & A_{1212} & A_{1213} & A_{1214} & A_{1215} & A_{1216} & A_{1217} \\ 0 & A_{132} & 0 & 0 & 0 & 0 & 0 & 0 & 0 & 0 & 0 & 0 & A_{1313} & A_{1314} & A_{1315} & 0 & 0 \\ 0 & A_{142} & 0 & 0 & 0 & 0 & 0 & 0 & 0 & 0 & 0 & 0 & 0 & A_{1414} & A_{1415} & 0 & 0 \\ 0 & A_{152} & 0 & 0 & 0 & 0 & 0 & 0 & 0 & 0 & 0 & 0 & 0 & 0 & A_{1515} & 0 & 0 \\ A_{161} & A_{162} & A_{163} & A_{164} & 0 & 0 & 0 & 0 & 0 & 0 & 0 & 0 & 0 & 0 & 0 & A_{1616} & A_{1617} \\ A_{171} & A_{172} & A_{173} & A_{174} & 0 & 0 & 0 & 0 & 0 & 0 & 0 & 0 & 0 & 0 & 0 & 0 & A_{1717} \end{vmatrix}. \quad \text{(A.1)}$$

where, $A_{12} = W_0$ $A_{21} = -(K_1/M)$, $A_{22} = -(D/M)$, $A_{23} - (K_2/M)$, $A_{27} = 1/M$, $A_{31} - (K_4/T_{d0}')$, $A_{33} = -(K_3/T_{d0}')$, $A_{34} = 1/T_{d0}'$, $A_{41} = -(K_5K_a/T_a)$, $A_{43} = -(K_6K_a/T_a)$, $A_{44} = -(1/T_a)$, $A_{46} = K_a/T_a$, $A_{51} = -K_1K_{ps}$, $A_{52} = -DK_{ps}$, $A_{53} = -K_2K_{ps}$, $A_{55} = -(1/T_W)$, $A_{57} = K_{ps}$, $A_{61} = -(K_1K_{ps}T_1/T_2)$, $A_{62} = -(DK_{ps}T_1/T_2)$, $A_{63} = -(K_2K_{ps}T_1/T_2)$, $A_{65} = 1/T_2$ $(1 - (T_1/T_W))$, $A_{66} = -(1/T_2)$, $A_{67} = K_{ps}T_1/T_2$, $A_{71} = (D_tY_0/M)K_1$, $A_{72} = D_tY_0((1/Z_2) + (D/M))$, $A_{73} = D_tY_0K_2/M$, $A_{77} = -((D_tY_0/M) - (1/Z_2))$, $A_{78} = -(A_t/Z_2)$ $(1 + (Z_1/t_a))$, $A_{79} = -A_t(Z_1/Z_2t_a)$, $A_{88} = -(1/t_a)$, $A_{89} = (1/t_a)$, $A_{910} = K_{sm}$, $A_{108} = -(K_C/T_C)$, $A_{1010} = -(1/T_C)$, $A_{1011} = K_C/T_C$, $A_{1012} = K_C/T_C$, $A_{1013} = K_CK_p/T_C$, $A_{1016} = -(K_CK_pR_P/T_C)$, $A_{1113} = K_i$, $A_{1116} = R_PK_i$, $A_{121} = R_PK_dK_{pe}K_2K_1T_{e1}/T_dT_{do}'T_{e2}$, $A_{122} = (K_d/T_d)$ $((R_PK_{pe}K_1T_{e1}\omega_0/T_{e2}) - (T_{P1}K_w/(0.05)T_{P2}))$, $A_{123} = -(R_PK_dK_{pe}K_2K_3/T_dT_{do}')$, $A_{124} = R_PK_dK_{pe}K_2T_{e1}/T_dT_{do}'T_{e2}$, $A_{1212} = -(1/T_d)$, $A_{1213} = -(K_d/T_d)$, $A_{1214} = (K_d/T_d)(1 - (T_{P1}/T_{P2}T_w))$, $A_{1215} = -(K_dK_wT_{p1}/(0.05)T_dT_{p2})$, $A_{1216} = -(R_PK_d/T_dT_{e2})$, $A_{1217} = 1 - (R_PK_dK_{pe}T_{e1}/T_dT_wT_{e2})$, $A_{132} = -(K_wT_{p1}/(0.05)T_{p2})$, $A_{1313} = -(1/T_{p2})$, $A_{1314} = -((1/T_W)(T_{p1}/T_{p2}) + (1/T_{p2}))$, $A_{1315} = -((T_{p1}/T_{p2})(K_w/0.05))$, $A_{142} = -(K_w/0.05)$, $A_{1414} = -(1/T_W)$, $A_{1415} = -(K_w/0.05)$, $A_{152} = -(1/0.05)$, $A_{1515} = -(1/0.05)$, $A_{161} = -((K_{pe}K_2K_4/T_{do}')(T_{e1}/T_{e2}))$, $A_{162} = K_{pe}K_1\omega_0$ (T_{e1}/T_{e2}), $A_{163} = -((K_{pe}K_2K_3/T_{do}')(T_{e1}/T_{e2}))$, $A_{164} = (K_{pe}K_2/T_{do}')(T_{e1}/T_{e2})$, $A_{1616} = -(1/T_{e2})$, $A_{1617} = (1/T_{e2})$ $((T_{e1}/T_W) + 1)$, $A_{171} = -(K_2K_4K_{pe}/T_{do}')$, $A_{172} = K_pK_1\omega_0$, $A_{173} = -(K_3K_{pe}K_2/T_{do}')$, $A_{174} = K_{pe}K_2/T_{do}'$, $A_{1717} = -(1/T_w)$.

Data Availability

The Ratings of machines and system under study data used to support the findings of this study are included within the article as appendix.

Conflicts of Interest

The authors declare that they have no conflicts of interest.

Acknowledgments

This work has been carried out at the energy center laboratory of our university Siksha O Anusandhan deemed to be University, Bhubaneswar, Odisha, India.

References

[1] X. Xiong and X. Ruan, "Non-smooth bifurcation analysis of multi-structure multi-operating-mode power electronics systems for applications with renewable energy sources," *In IEEE Transactions on Circuits and Systems II: Express Briefs*, vol. 3, pp. 487–491, 2018.

[2] M. Numan, D. Feng, F. Abbas, S. Habib, and A. Rasool, "Mobilizing grid flexibility through optimal transmission switching for power systems with large-scale renewable integration," *International Transactions on Electrical Energy Systems*, vol. 30, no. 3, 2020.

[3] T. Ma, W. Gu, L. Shen, and M. Li, "An improved and comprehensive mathematical model for solar photovoltaic modules under real operating conditions," *Solar Energy*, vol. 184, pp. 292–304, 2019.

[4] W. Yang, P. Norrlund, L. Saarinen et al., "Burden on hydropower units for short-term balancing of renewable power systems," *Nature Communications*, vol. 9, no. 1, pp. 2633–2712, 2018.

[5] B. Dunn, H. Kamath, and J.-M. Tarascon, "Electrical energy storage for the grid: a battery of choices," *Science*, vol. 334, no. 6058, pp. 928–935, 2011.

[6] D. Sprake, Y. Vagapov, S. Lupin, and A. Anuchin, "Housing estate energy storage feasibility for a 2050 scenario," in *Proceedings of the 2017 Internet Technologies and Applications (ITA)*, Wrexham, UK, 2017.

[7] S. Q. Bu, W. Du, H. F. Wang, Z. Chen, L. Y. Xiao, and H. F. Li, "Probabilistic analysis of small-signal stability of large-scale power systems as affected by penetration of wind generation," *IEEE Transactions on Power Systems*, vol. 27, no. 2, pp. 762–770, 2012.

[8] J. G. Slootweg and W. L. Kling, "The impact of large scale wind power generation on power system oscillations," *Electric Power Systems Research*, vol. 67, no. 1, pp. 9–20, 2003.

[9] J. J. Sanchez-Gasea, N. W. Miller, and W. W. Price, "A modal analysis of a two-area system with significant wind power penetration," in *Proceedings of the Power Systems Conference and Exposition*, New York, NY, USA, 2004.

[10] S. Lamichhane and N. Mithulanananthan, "Possible impact of large scale wind energy integration on small signal stability," in *Proceedings of the IEEE PES Asia-Pacific Power and Energy Engineering Conference (APPEEC)*, Brisbane, QLD, Australia, 2015.

[11] W. Liu, R. Ge, H. Li, and J. Ge, "Impact of large-scale wind power integration on small signal stability based on stability region boundary," *Sustainability*, vol. 6, no. 11, pp. 7921–7944, 2014.

[12] Y. T. Tan, D. S. Kirschen, and N. Jenkins, "A model of PV generation suitable for stability analysis," *IEEE Transactions on Energy Conversion*, vol. 19, no. 4, pp. pp748–755, 2004.

[13] L. Wang and T. Lin, "Dynamic stability and transient responses of multiple grid-connected PV systems," in *Proceedings of the IEEE/PES Transmission and Distribution Conference and Exposition*, Chicago, IL, 2008.

[14] T. Shimizu, M. Hirakata, T. Kamezawa, and H. Watanabe, "Generation control circuit for photovoltaic modules," *IEEE Transactions on Power Electronics*, vol. 16, pp. 293–300, 2001.

[15] H. Matsuo and F. Kurokawa, "Novel solar cell power supply system using bidirectional DC-DC converter," *IEEE Transactions on Industrial Electronics*, vol. 53, pp. 14–19, 1982.

[16] W. Du, H. F. Wang, and R. Dunn, "Power system small-signal oscillation stability as affected by large-scale PV penetration," in *Proceedings of the International Conference on Sustainable Power Generation And Supply*, Nanjing, China, 2009.

[17] S. Eftekharnejad, V. Vittal, G. T. Heydt, B. Keel, and J. Loehr, "Small signal stability assessment of power systems with increased penetration of photovoltaic generation: a case study," *IEEE Transactions on Sustainable Energy*, vol. 4, no. 4, pp. 960–967, 2013.

[18] D.-J. Lee and L. Wang, "Small-signal stability analysis of an autonomous hybrid renewable energy power generation/energy storage system Part I: time-domain simulations," *IEEE Transactions on Energy Conversion*, vol. 23, no. 1, pp. 311–320, 2008.

[19] N. Nahak and R. K. Mallick, "Investigation and damping of low-frequency oscillations of stochastic solar penetrated power system by optimal dual UPFC," *IET Renewable Power Generation*, vol. 13, pp. 376–388, 2019.

[20] M. Rahmatian and S. Seyedtabaii, "Multi-machine optimal power system stabilizers design based on system stability and nonlinearity indices using Hyper-Spherical Search method," *International Journal of Electrical Power & Energy Systems*, vol. 105, pp. 729–740, 2019.

[21] S. Yang, L. Xiong, S. Huang et al., "Optimal node selection of damping controller for power systems with high wind power penetration," *International Journal of Electrical Power & Energy Systems*, vol. 136, Article ID 107716, 2022.

[22] H. F. Wang, Y. S. Hao, B. W. Hogg, and Y. H. Yang, "Stabilization of power systems by governor—turbine control," *International Journal of Electrical Power & Energy Systems*, vol. 15, no. 6, pp. 351–361, 1993.

[23] Working Group on Prime Mover and Energy Supply, "Hydraulic turbine and turbine control models for system dynamic studies," *IEEE Transactions on Power Systems*, vol. 7, no. 1, pp. 167–179, 1992.

[24] S. K. Yee, J. V. Milanovic, and F. M. Hughes, "Damping of system oscillatory modes by a phase compensated gas turbine governor," *Electric Power Systems Research*, vol. 80, no. 6, pp. 667–674, 2010.

[25] *Report on Low Frequency Oscillation in Indian Power System*, Power System Operation Corporation Limited, New Delhi, India, 2016.

[26] G. Kenné, A. M. Fombu, and J. d. D. Nguimfack-Ndongmo, "Coordinated excitation and steam valve control for multimachine power system using high order sliding mode technique," *Electric Power Systems Research*, vol. 131, pp. 87–95, 2016.

[27] M. Elsisi and M. A. Ebrahim, "Optimal design of low computational burden model predictive control based on SSDA towards autonomous vehicle under vision dynamics," *International Journal of Intelligent Systems*, vol. 36, no. 11, pp. 6968–6987, 2021.

[28] M. Elsisi, M.-Q. Tran, H. M. Hasanien, R. A. Turky, F. Albalawi, and S. S. M. Ghoneim, "Robust model predictive control paradigm for automatic voltage regulators against uncertainty based on optimization algorithms," *Mathematics*, vol. 2885, no. 9, 2021.

[29] M. Elsisi and H. Abdelfattah, "New design of variable structure control based on lightning search algorithm for nuclear reactor power system considering load-following operation," *Nuclear Engineering and Technology*, vol. 52, no. 3, 2020.

[30] M. Elsisi, "New design of robust PID controller based on meta-heuristic algorithms for wind energy conversion system," *Wind Energy*, vol. 23, no. 2, pp. 391–403, 2020.

[31] Y. Arya and K. Narendra, "Fuzzy gain scheduling controllers for automatic generation control of two-area interconnected electrical power systems," *Electric Power Components and Systems*, vol. 44, 2016.

[32] Y. Arya, N. Kumar, and Ibraheem, "AGC of a two-area multisource power system interconnected via AC/DC parallel links under restructured power environment," *Optimal Control Applications and Methods*, vol. 37, no. 4, pp. 590–607, 2016.

[33] G. Sharma, A. Panwar, Y. Arya, and M. Kumawat, "Integrating layered recurrent ANN with robust control strategy for diverse operating conditions of AGC of the power system," *IET Generation, Transmission & Distribution*, vol. 14, no. 18, pp. 3886–3895, 2020.

[34] M. Sharma, S. Dhundhara, Y. Arya, and S. Prakash, "Frequency stabilization in deregulated energy system using coordinated operation of fuzzy controller and redox flow battery," *International Journal of Energy Research*, vol. 45, no. 5, pp. 7457–7475, 2021.

[35] M. Sharma, S. Dhundhara, Y. Arya, and S. Prakash, "Frequency excursion mitigation strategy using a novel COA optimised fuzzy controller in wind integrated power systems," *IET Renewable Power Generation*, vol. 14, no. 19, pp. 4071–4085, 2020.

[36] D. K. Sahoo, R. K. Sahu, G. T. Chandra Sekhar, and S. Panda, "A novel modified differential evolution algorithm optimized fuzzy proportional integral derivative controller for load frequency control with thyristor-controlled series compensator," *Journal of Electrical Systems and Information Technology*, vol. 5, 2017.

[37] W. Yang, P. Norrlund, C. Y. Chung, J. Yang, and U. Lundin, "Eigen-analysis of hydraulic-mechanical-electrical coupling mechanism for small signal stability of hydropower plant," *Renewable Energy*, vol. 115, pp. 1014–1025, 2018.

[38] I. Kamwa, D. Lefebvre, and L. Loud, "Small signal analysis of hydro-turbine governors in large interconnected power plants," in *2002 IEEE Power Engineering Society Winter Meeting*, New York, NY, USA, 2002.

[39] P. N. Suganthan, N. Hansen, J. J. Liang et al., "Problem definitions and evaluation criteria for the CEC 2005 special session on real parameter optimization," *Technical Report*, Nanyang Technological University, Singapore, 2005.